

Nitrosyliron complexes of macrocyclic $[N_4^{2-}]$ and open-chain $[N_2O_2^{2-}]$ chelate ligands: influence of the equatorial ligand on the NO binding mode

B. Weber, H. Görls, M. Rudolph, E.-G. Jäger*

Institute of Inorganic and Analytical Chemistry, Friedrich-Schiller-Universität Jena, August-Bebel-Str. 2, D-07743 Jena, Germany

Received 8 March 2002; accepted 7 June 2002

Dedicated to Karl Wieghardt on the occasion of his 60th birthday

Abstract

Several new nitrosyliron complexes $FeL-NO$ (L^{2-} : macrocyclic $[N_4]$ coordinated or open-chain $[N_2O_2]$ coordinated Schiff base ligand) were synthesised and compared with respect to their chemical behaviour (reactivity with dioxygen; redox potentials), their T -dependent magnetic susceptibility and their molecule structure. These properties reflect clearly the electronic influence of the equatorial chelate ligand (if present, also of an additional axial ligand) on the electron density at the central atom and, as a consequence, on the NO-binding mode. The macrocyclic complexes with the strongest equatorial donor ligands give pentacoordinated low spin ($S = 1/2$) derivatives, best to interpret as $[Fe^{III}L^+ - NO^-]$ —similar as the halides or pseudo-halides $FeL-X$. These complexes show no tendency to add additional axial ligands and are insensitive to air in non-coordinating solvents. In presence of a donor ligand D (pyridine, MeOH) the reaction with dioxygen results in an octahedral nitro derivative $FeL(NO_2) \times D$ that can also be prepared by reaction of the iron(III) complex $[FeL \times 2D]^+$ with sodium nitrite. This could be proved especially for the most electron-rich complex $Fe1-NO$ which can also be oxidised electrochemically in MeCN to give $[Fe1-NO]^+$ and $[Fe1-NO]^2+$ in two reversible steps. The $[N_2O_2]$ coordinated complexes with weaker donor ligands in the equatorial plane show a more differentiated behaviour depending on electronic effects of the peripheral ligand substituents. Octahedral adducts $FeL-NO \times D$ could be isolated from several of such complexes under anaerobic conditions. Their reaction with dioxygen gives the μ -oxo derivative $(FeL)_2O$ as the main product. Decreasing electron density at the central atom results in a trend towards decreasing transition temperature between a low-temperature $S = 1/2$ and a high-temperature $S = 3/2$ state. The atom distances within the first coordination sphere of the complex $Fe5-NO \times MeOH$ with the most electron withdrawing substitution of the equatorial ligand are significantly longer than those of the other complexes and show a surprising similarity to those of octahedral high-spin di-adducts $FeL \times 2D$ of the iron(II) complexes. This fact suggests an interpretation as $[Fe^{II}L-NO \times MeOH]$ with a coupling of the iron(II) $S = 4/2$ state with the unpaired electron of the NO radical. The electronic influence of the equatorial ligands is also reflected in a significant correlation between the angle Fe–N–O (varying from 140 to 167°) and the NO stretching frequencies (varying from 1629 to 1812 cm^{-1}).

© 2002 Elsevier Science B.V. All rights reserved.

Keywords: Iron; Nitrosyl complexes; Macrocycles; Cyclovoltammetry; Magnetic moment; Molecule structures

1. Introduction

There has been a renewed interest in the chemistry of nitric oxide (NO) during the last few years because of its role in biological systems. NO is a biological messenger in a wide range of physiological processes, it is essential

* Corresponding author

E-mail address: ernst-gottfried.jaeger@uni-jena.de (E.-G. Jäger).

in host defence and immunological reactions and responsible for the colour and stability of cured meats [1,2]. Nitric oxide is synthesised *in vivo* by the hem enzyme nitric oxide synthase by stepwise oxidation of L-arginine to NO and L-citrulline [1,2] and it is also an intermediate in the reduction of nitrite to ammonia by the hem enzyme nitrite reductase [3].

The groundwork relating to current studies was laid about three decades ago when NO has been used as EPR active probe for studying the reaction of hem proteins and related derivatives with small molecules [4,5]. The reaction of nitric oxide with ferrous and ferric porphyrins in the presence or absence of additional axial ligands and the formed nitrosyl complexes have been investigated in detail using X-ray absorption, EPR, Mössbauer, IR and UV–Vis spectroscopy [6]. In addition NO-adducts of several non-porphyrin iron chelate complexes as tetramethylcyclam, phthalocyanine and quadridentate Schiff bases ligands, have been prepared and spectroscopically characterised. Some of them exhibit $S = 3/2$ ground states or low spin ($S = 1/2$) \leftrightarrow intermediate spin ($S = 3/2$) transitions [7]. The dependence of the M–N–O geometry of the number of electrons determined by the electron-counting formalism of Enemark and Feltham [8] has been discussed in various cases [6,7,9]. Selected structural, IR- and magnetic data of several known nitrosyliron complexes are listed in Table 1.

Despite the enormous number of known nitrosyliron complexes with porphyrins and related anionic equatorial ligands, up to now there have been surprisingly few systematic investigations on relationships between the electronic properties of the equatorial ligand and the

binding conditions of the NO to the iron. This is an important question because in biological systems the equatorial ligand together with the protein controls the electronic (and geometric) features of the active site and the reactivity of the iron towards the binding and activation of small molecules, their precursors, and their metabolites.

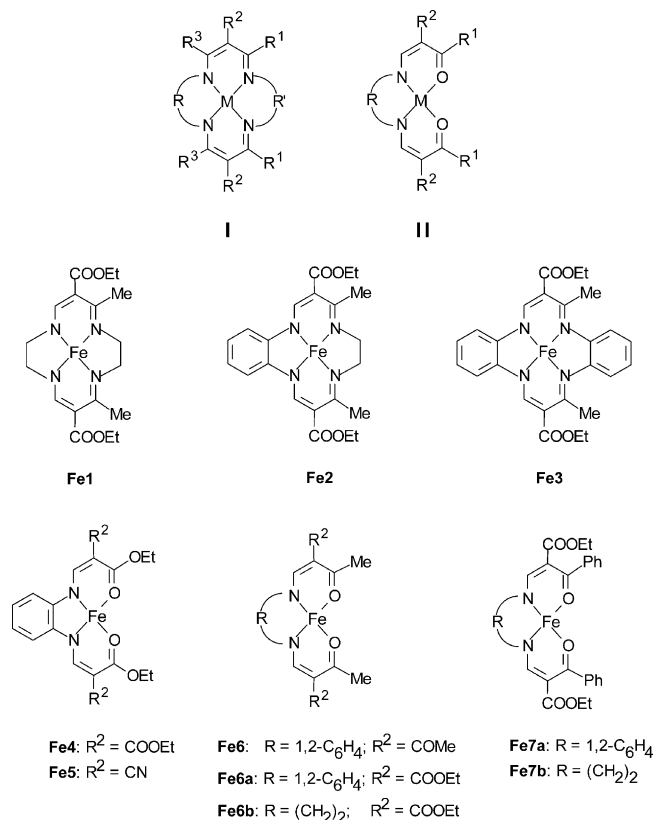
In this paper, we present the synthesis and characterisation of ‘{FeNO}⁷⁺’ nitrosyliron complexes with dianionic tetradentate chelate ligands derived either from macrocyclic [N₄] coordinated bis(3-imino-enamines) (type I) or from open-chain [N₂O₂] coordinated bis(3-oxo-enamines) (type II). The advantage of these ligands is their broad variability. Former investigations of copper [11,12b], nickel [12b,13,14], cobalt [12b,13,15] and iron complexes [12,13,16] type I and II showed the principal possibility to control such properties as the affinity of vacant axial coordination sites towards additional ligands, the reduction and oxidation potentials, the binding and activation of dioxygen [15] or carbon dioxide [17], the magnetic behaviour and special structural features by use of electronic (and in part steric) effects of the bridges R, R’ and the peripheral substituents R¹ and R² (with a few exceptions, R³ is H in our complexes). The formula of the base iron(II) complexes and their abbreviations used in this paper are given in Scheme 1. The aim of our studies is to gain information on the NO binding mode in the complexes FeL–NO by comparison of their typical properties—such as UV–Vis and IR spectra, reactivity with additional axial ligands and stability on air, the redox behaviour, the spin state and the molecule structure—with those of the corresponding base complexes FeL. Prior to our

Table 1
Several known nitrosyliron complexes

Complex ^a	$d_{M-N(NO)}$ (Å)	d_{M-L} (Å)	$\angle MNO$ (°)	d_{N-O} (Å)	ν_{NO} (cm ⁻¹)	S	Reference
‘{FeNO} ⁷⁺ ’ ^b							
[Fe(TPP)NO]	1.717		149.2	1.122	1670	1/2	[6]
[Fe(OEP)NO] (monoclinic)	1.722		144.4	1.167	1666		[6]
[Fe(TMC)NO](BF ₄) ₂	1.737		177.5	1.137	1840	1/2 \leftrightarrow 3/2	[7b]
[Fe(Me ₄ TAA)NO]	1.716		144.1	1.17	1636	1/2	[7c]
[Fe(Salen)NO] (1)	1.783		144, 150	1.11	1710	3/2	[7d,10]
[Fe(Salen)NO] (2)	1.80		122, 132	1.15	1630	1/2	[7d,10]
[Fe(TPP)NO(1MeIm)]	1.743	2.180	142.1	1.121	1625		[6]
[Fe(T _{piv} PP)NO(NO ₂)] ⁻ (average of 3 values)	1.802	2.075	138.1	1.155	1616, 1668		[6]
‘{FeNO} ⁶⁺ ’ ^b							
[Fe(OEP)NO] ⁺	1.644		176.9	1.112	1862	0	[6]
[Fe(TPP)NO(H ₂ O)] ⁺	1.652	2.001	174.4	1.150	1937	0	[6]
[Fe(OEP)NO(1MeIm)] ⁺	1.6465	1.9889	177.28	1.135	1921		[6]

^a Abbreviations used in this paper: TPP, tetraphenylporphyrin, OEP, octaethylporphyrin, TMC, tetramethyl-tetraaza-cyclotetradecan, Me₄TAA, tetramethyl-dibenzotetraaza-[14]annulen, Salen, bis-salicylaldehyde-ethylenediimin, T_{piv}PP, tetra(pivaloylphenyl)-porphyrin; Him, imidazole, MeOH, methanol, Py, pyridine, DMF, dimethylformamide.

^b Designation after Enemark and Feltham [8].



Scheme 1. Abbreviations of iron(II) complexes used as starting material for nitrosyl derivatives.

work the complex **Fe6–NO** was synthesised by Numata et al. [18] and later investigated magnetically by König et al. [7e]. The NO derivative of the iron complex type **I** with R = R' = 1,2-phenylene, R¹ = R³ = Me and R² = H (**FeMe₄TAA**) was earlier synthesised and structurally characterised by Floriani et al. [7c].

2. Experimental

2.1. General procedures and instrumentation

The solvents methanol, toluene and pyridine were purified as described in the literature [18].

Infrared measurements were performed in the range of 4000–650 cm⁻¹ with a Perkin–Elmer System 2000 FT IR-Spectrometer as Nujol mulls at room temperature (r.t.). The NO-stretching frequency was obtained by comparison of the infrared spectra of the NO-adduct with the IR spectra of the corresponding iron(II) complex and iron(III) halide complex. In most cases—with the exception of **Fe7b–NO**—the position of the NO-stretching frequency could be determined clearly.

Electronic spectra were measured with a Varian Cary 5 spectrophotometer at r.t. using methanol, toluene and pyridine as solvents.

Magnetic measurements of powered samples were performed on a Quantum-Design-MPMSR-5s-SQUID-Magnetometer in a temperature range from 1.7 to 300 K. All measurements were carried out at two field strength (0.2 and 0.5 T). No significant field dependence was observed. Diamagnetic corrections were made by using the molar susceptibilities of the analogous diamagnetic nickel(II) complexes without NO. They are in satisfactory agreement with the values calculated with tabulated Pascal constants (as a rule, suitable values can be estimated as $\chi_{\text{dia}} \approx 0.6 \times 10^{-6} \text{ M}_{\text{complex}}$).

Mass spectroscopic investigations were performed using a SSQ 710 or a MAT95XL mass spectrometer and direct electron beam ionisation as stimulation.

2.2. Syntheses

2.2.1. Iron(II) complexes

The iron(II) complexes **Fe1** [12a], **Fe2** [12b], **Fe3** [20], **Fe4** × 2Py, **Fe5** × 3Py, **Fe6** × 2MeOH, **Fe6a**, **Fe7a** × 2Py [16a] and the ligands **H₂1** [21], **H₂7a**, [14a] and **H₂7b** [14a,21] have been prepared as described in the literature. All preparations were done using Schlenk techniques and argon as inert gas [19].

Fe7a × 2MeOH. ([*E,E*]-[diethyl 2,2'-1,2-phenylenebis(iminomethylidene)bis(3-oxo-3-phenylpropanato)](2-)-*N,N',O³,O^{3'}*]iron(II)): 2 methanol: 1.7 g (9.9 mmol) iron(II)acetate and 4.24 g (8.3 mmol) **H₂7a** were dissolved in 50 ml methanol and heated to reflux for 1 h. After cooling down, the black precipitate was filtered off and dried in vacuo. Yield: 4.3 g (91%). *Anal.* Calc. for C₃₀H₂₆N₂O₆Fe × 2CH₃OH: C, 60.96; H, 5.44; N, 4.44; Fe, 9.86. Found: C, 57.04; H, 4.53; N, 4.33; Fe, 9.73%. IR (Nujol): $\nu_{\text{C=O}} = 1691 \text{ cm}^{-1}$. MS (DEI): Base peak: 105 *m/z* (fragment; 100%); 566 *m/z* (M⁺, 50%).

Fe7b × 2Py ([*E,E*]-[diethyl-2,2'-1,2-ethylenebis(iminomethylidene)bis(3-oxo-3-phenylpropanato)](2-)-*N,N',O³,O^{3'}*]iron(II)) × 2pyridine: 2.0 g (11.4 mmol) iron(II)acetate, 4.1 g (8.8 mmol) **H₂7b** and 2.32 g (34.2 mmol) sodiummethanolate were dissolved in 30 ml methanol and 30 ml pyridine and heated to reflux for 1 h. The solution was left in the freezer over night to yield bright to dark red crystals, which were collected, washed with a little amount of methanol and dried in vacuo. Yield: 2.84 g (63%). *Anal.* Calc. for C₂₆H₂₆N₂O₆Fe × 2C₅H₅N: C, 63.91; H, 5.36; N, 8.28. Found: C, 62.73; H, 5.29; N, 8.15%. IR (Nujol): $\nu_{\text{C=O}} = 1671 \text{ cm}^{-1}$. MS (DEI): Base peak: 79 *m/z* (Pyridine; 100%); 518 *m/z* (M⁺, 30%); 473 *m/z* (M⁺–OCH₂CH₃, 10%).

2.2.2. Nitrosyl derivatives

2.2.2.1. General procedure. Nitric oxide (formed and purified according to Dickinson et al. [22]) was bubbled through a solution (**Fe1**, **Fe6**, **Fe6a**) or suspension (**Fe2**, **Fe3**, **Fe4**, **Fe5**, **Fe7a**, **Fe7b**) of the corresponding iron(II)

complex. The formed product was filtered off and dried in vacuo.

Fe1–NO ((6,13-bis(ethoxycarbonyl)-7,12-dimethyl-1,4,8,11-tetraazacyclotetradeca-5,7,12,14-tetraenoato(2-))nitrosyliron(II)): 1.09 g (6.2 mmol) iron(II)acetate and 2.17 g (5.9 mmol) ligand **H₂1** were dissolved in 50 ml MeOH and heated to reflux for 1 h. After cooling down nitric oxide was bubbled through the solution. The colour of the solution changed from red to green and the product precipitates immediately. The precipitate was collected and dried in vacuo. The mother solution was allowed to stand over night to produce single crystals of **Fe1–NO** suitable for X-ray crystallography. Yield: 1.85 g (69%). *Anal.* Calc. for C₁₈H₂₆N₅O₅Fe: C, 48.25; H, 5.85; N, 15.64; Fe, 12.46. Found: C, 45.21; H, 5.40; N, 13.84; Fe, 12.28%. IR (Nujol) $\nu_{\text{NO}} = 1629 \text{ cm}^{-1}$. MS (DEI): Base peak: 418 *m/z* (M⁺–NO, 100%); 30 *m/z* (NO⁺, 15%), 448 *m/z* (M⁺, 10%).

Fe2–NO (6,13-bis(ethoxycarbonyl)-7,12-dimethylbenzo-[b,i]-1,4,8,11-tetraazacyclotetradeca-5,7,12,14-tetraenoato(2-))nitrosyliron(II)): 0.19 g (0.4 mmol) **Fe2** were suspended in 20 ml MeOH and nitric oxide was bubbled through the suspension for half an hour. The crystalline product was filtered off and dried in vacuo. To obtain single crystals suitable for X-ray crystallography some of the product was slowly crystallised from a pyridine–methanol solution. Yield: 0.16 g (75%). *Anal.* Calc. for C₂₂H₂₆N₅O₅Fe: C, 53.24; H, 5.28; N, 14.11. Found: C, 52.15; H, 5.02; N, 13.96%. IR (Nujol) $\nu_{\text{N=O}} = 1637 \text{ cm}^{-1}$. MS (DEI): Base peak: 30 *m/z* (NO⁺, 100%); 466 *m/z* (M⁺–NO, 80%); 496 *m/z* (M⁺, 5%).

Fe3–NO (6,13-bis(ethoxycarbonyl)-7,12-dimethyl-dibenzo-[b,i]-1,4,8,11-tetraazacyclotetradeca-5,7,12,14-tetraenoato(2-))nitrosyliron(II)): 0.23 g (0.5 mmol) **Fe3** were suspended in 30 ml MeOH and nitric oxide was bubbled through the solution for half an hour. The crystalline product was filtered off and dried in vacuo. Yield: 0.22 g (80%). *Anal.* Calc. for C₂₆H₂₆N₅O₅Fe: C, 57.36; H, 4.81; N, 12.87. Found: C, 54.32; H, 4.31; N, 10.72%. IR (Nujol) $\nu_{\text{N=O}} = 1675 \text{ cm}^{-1}$. MS (DEI): Base peak: 514 *m/z* (M⁺–NO, 100%); 30 *m/z* (NO⁺, 80%), 544 *m/z* (M⁺, 5%).

Fe4–NO × MeOH ((*E,E*)-[tetraethyl 2,2'-{1,2-phenylenebis(iminomethylidene)} bis-(propanodiato)(2-)*N,N',O⁴,O⁴*]-nitrosyliron) × MeOH: 0.4 g (0.8 mmol) **Fe4** × **2Py** were suspended in 20 ml MeOH. Nitric oxide was bubbled through the suspension till a clear solution was obtained. The solution was left in the freezer to yield dark brown crystals. Yield: 0.26 g (63%). *Anal.* Calc. for C₂₃H₃₀N₃O₁₀Fe: C, 48.94; H, 5.36; N, 7.45. Found: C, 49.10; H, 5.43; N, 7.21%. IR (Nujol) $\nu_{\text{N=O}} = 1716 \text{ cm}^{-1}$. MS (DEI): Base peak: 30 *m/z* (NO⁺, 100%); 502 *m/z* (M⁺–NO, 5%).

Fe5–NO × MeOH(1) ((*Z,Z*)-[diethyl 3,3'-(1,2-phenylenediimino) bis(2-cyano-2-propenoato)](2-)-

N³,N^{3'},O¹,O^{1'}]-nitrosyliron) × MeOH: 0.47 g (0.7 mmol) **Fe5** × **3Py** were suspended in 50 ml MeOH. Nitric oxide was bubbled through the suspension till a clear solution was obtained. The solution was left in the freezer to yield black crystals. Yield: 0.13 g (39%). *Anal.* Calc. for C₁₉H₂₀N₅O₆Fe: C, 48.53; H, 4.29; N, 14.89. Found: C, 47.72; H, 4.11; N, 14.35%. IR (Nujol) $\nu_{\text{N=O}} = 1744 \text{ cm}^{-1}$. MS (DEI): Base peak: 30 *m/z* (NO⁺, 100%); 408 *m/z* (M⁺–NO, 70%).

Fe5–NO × MeOH(2): The same procedure carried out at –78 °C (dry ice CO₂–ethanol) yielded black crystals which rearranged quickly into the above product at r.t. The identity of these crystals was proved by X-ray analysis, but it was not possible to measure the characteristic IR using standard methods.

Fe5–NO ((*Z,Z*)-[diethyl 3,3'-(1,2-phenylenediimino) bis(2-cyano-2-propenoato)](2-)-*N³,N^{3'},O¹,O^{1'}*]-nitrosyliron): 0.81 g (1.3 mmol) **Fe5** × **3Py** were suspended in 50 ml MeOH. Nitric oxide was bubbled through the suspension for one and a half hour. The microcrystalline product was filtered off and dried in vacuo. Yield: 0.49 g (85%). *Anal.* Calc. for C₁₈H₁₆N₅O₅Fe: C, 49.33; H, 3.68; N, 15.98. Found: C, 48.09; H, 3.75; N, 15.13%. IR (Nujol) $\nu_{\text{N=O}} = 1812 \text{ cm}^{-1}$. MS (DEI): Base peak: 30 *m/z* (NO⁺, 100%); 408 *m/z* (M⁺–NO, 5%).

Fe6–NO ([3,3']-[1,2-phenylenebis(iminomethylidene) bis(2,4-pentanedionato)(2-)-*N,N',O²,O²*]-nitrosyliron): Nitric oxide was bubbled through a solution of 1.1 g (2.88 mmol) **Fe6** × **2MeOH** in 100 ml methanol. The precipitate was filtered off and dried in vacuo. Yield: 0.94 g (79%). *Anal.* Calc. for C₁₈H₁₈N₃O₅Fe: C, 52.45; H, 4.40; N, 10.20. Found: C, 52.36; H, 4.30; N, 10.10%. IR (Nujol) $\nu_{\text{N=O}} = 1790 \text{ cm}^{-1}$. MS (DEI): Base peak: 30 *m/z* (NO⁺, 100%); 412 *m/z* (M⁺, 1%); 382 *m/z* (M⁺–NO, 15%).

Fe6a–NO (Diethyl-2,2'-[1,2-phenylene-bis(iminomethylidene) bis(3-oxo-butanoato)(2-)-*N,N',O³,O³*]-nitrosyliron): Nitric oxide was bubbled through a solution of 0.1 g (0.2 mmol) **Fe6a** × **2MeOH** in 15 ml methanol. The precipitate was filtered off and dried in vacuo. Yield: 0.08 g (85%). *Anal.* Calc. for C₂₀H₂₂N₃O₇Fe: C, 50.86; H, 4.69; N, 8.90. Found: C, 52.73; H, 5.01; N, 8.11%. IR (Nujol) $\nu_{\text{N=O}} = 1776 \text{ cm}^{-1}$, MS (DEI): Base peak: 442 *m/z* (M⁺–NO, 100%); 30 *m/z* (NO⁺, 100%).

Fe7a–NO ([*E,E*]-[diethyl-2,2'-1,2-phenylene-bis(iminomethylidene) bis(3-oxo-3-phenylpropanoato)](2-)-*N,N',O³,O³*]-nitrosyliron): Nitric oxide was bubbled through a suspension of 0.75 g (1.3 mmol) **Fe7a** × **2MeOH** in 60 ml MeOH for 1 h. The black fine crystalline product was filtered off and dried in vacuo. Yield: 0.63 g (84%) *Anal.* Calc. for C₃₀H₂₆N₃O₇Fe: C, 60.41; H, 4.39; N, 7.05. Found: C, 59.78; H, 4.43; N, 6.96%. IR (Nujol) $\nu_{\text{N=O}} = 1778 \text{ cm}^{-1}$. MS (DEI): Basis peak: 566 *m/z* (M⁺–NO, 100%); 30 *m/z* (NO, 80%); 521 *m/z* (M⁺–NO–OCH₂CH₃, 20%).

Fe7b–NO (*[E,E]*-[diethyl 2,2'-1,2-ethylenebis(imino-methylidene)bis(3-oxo-3-phenylpropanoato)](2-)-*N,N',O³,O³*]-nitrosyliron): Nitric oxide was bubbled through a suspension of 1.7 g (2.5 mmol) **Fe7b** × **2Py** in 30 ml methanol until a clear solution was obtained. The solution was left in the freezer over night to yield a fine crystalline black product that was filtered off and dried in vacuo. Yield: 0.69 g (52%). *Anal. Calc.* for C₂₆H₂₆N₃O₇Fe: C, 56.95; H, 4.78; N, 7.66. Found: C, 56.75; H, 4.67; N, 7.34%. IR (Nujol) $\nu_{\text{N=O}}$, $\nu_{\text{C=O}}$: 1700, 1696, 1659, 1655 cm⁻¹. MS (DEI): Base peak: 30 *m/z* (NO⁺, 100%); 518 *m/z* (M⁺–NO, 60%).

2.3. Electrochemistry

Cyclic and square wave voltammetric measurements have been conducted in 3-electrode technique using a home-built computer controlled instrument based on the PCI-MIO-16E-1 data acquisition board (National Instruments). The experiments were performed either in methylenechloride or in acetonitrile containing 0.5M tetra-*n*-butylammonium-perchlorate under a blanket of solvent-saturated argon. The complex concentration was about 0.015 m in all experiments. The ohmic resistance, which had to be compensated for, was determined by measuring the impedance of the system at potentials where the Faradaic current was negligibly small. Background correction was accomplished by subtracting the current curves of the blank electrolyte (containing the same concentration of supporting electrolyte) from the experimental CVs. The reference electrode was Ag/AgCl in acetonitrile containing 0.25 M tetra-*n*-butylammonium chloride (abbreviated 'Ag'). The potential of this reference system was calibrated by measuring the potential of the ferrocene–ferricinium couple at the end of each experiment. The latter was found to be at 0.855 ± 0.002 V in methylenechloride and +0.785 ± 0.001 V in acetonitrile, respectively. Calibration using the complex Ni1—the potentials of which versus SCE ($E_{\text{H}} = 0.241$ V) are nearly independent from the solvents MeCN, DMF, and pyridine [16f]—leads to a potential of $E_{\text{H}}(\text{'Ag'}) - 0.163$ V in MeCN and -0.237 V in methylenechloride for this electrode. The working electrode was either an hanging mercury drop ($m_{\text{Hg-drop}} = 3.95\text{--}4$ mg) produced by the CGME instrument or a 1.5 mm Pt disk electrode (both from Bioanalytical Systems, Inc., West Lafayette, USA).

2.4. X-ray crystallography

2.4.1. Crystal structure determination

The intensity data for the compounds were collected on a Nonius κCCD diffractometer, using graphite-monochromated Mo Kα radiation. Data were corrected for Lorentz and polarisation effects, but not for absorption [23,24].

The structures were solved by direct methods (SHELXS [25]) and refined by full-matrix least-squares techniques against F_o^2 (SHELXL-97 [26]). The quality of the data of compound **Fe6–NO** is too bad. We will only be publishing the conformation of the molecule and the crystallographic data. We will not deposit the data in the Cambridge Crystallographic Data Centre. For the compound **Fe5–NO** × **MeOH(1)** all hydrogen atoms were located by difference Fourier synthesis and refined isotropically. For the compound **Fe4–NO** × **MeOH** only the hydrogen atom of the hydroxy-group of the methanol was located by difference Fourier synthesis and refined isotropically. The other hydrogen atoms were included at calculated positions with fixed thermal parameters. All non-hydrogen atoms were refined anisotropically [26]. XP (SIEMENS Analytical X-ray Instruments, Inc.) was used for structure representations.

2.4.2. Crystal data for **Fe1–NO**

C₁₈H₂₆FeN₅O₅, $M_r = 448.29$ g mol⁻¹, brown prism, size 0.22 × 0.20 × 0.12 mm, triclinic, space group $P\bar{1}$, $a = 10.0030(5)$, $b = 10.3890(5)$, $c = 10.8640(5)$ Å; $\alpha = 103.017(3)$, $\beta = 109.871(3)$, $\gamma = 94.539(3)^\circ$; $V = 1019.45(8)$ Å³, $T = -90$ °C, $Z = 2$, $\rho_{\text{calc}} = 1.460$ g cm⁻³, μ (Mo Kα) = 7.8 cm⁻¹, $F(000) = 470$, 6788 reflections in $h(-12/10)$, $k(-12/13)$, $l(-12/13)$, measured in the range $3.24 \leq \theta \leq 27.35^\circ$, completeness $\Theta_{\text{max}} = 97.2\%$, 4488 independent reflections, $R_{\text{int}} = 0.031$, 3588 reflections with $F_o > 4\sigma(F_o)$, 272 parameters, 0 restraints, $R_{\text{obs}}^1 = 0.054$, $wR_{\text{obs}}^2 = 0.120$, $R_{\text{obs}}^1 = 0.076$, $wR_{\text{obs}}^2 = 0.131$, GOOF = 1.011, largest difference peak and hole: 0.601/–0.489 e Å⁻³.

2.4.3. Crystal data for **Fe2–NO**

C₂₂H₂₆FeN₅O₅, $M_r = 496.33$ g mol⁻¹, brown or green prism, size 0.12 × 0.10 × 0.09 mm, monoclinic, space group $P2_1/n$, $a = 7.6622(2)$, $b = 13.8944(5)$, $c = 20.4088(5)$ Å; $\beta = 95.048(2)^\circ$, $V = 2164.33(11)$ Å³, $T = -90$ °C, $Z = 4$, $\rho_{\text{calc}} = 1.523$ g cm⁻³, μ (Mo Kα) = 7.43 cm⁻¹, $F(000) = 1036$, 8555 reflections in $h(-9/9)$, $k(-18/16)$, $l(-26/26)$, measured in the range $2.93 \leq \theta \leq 27.47^\circ$, completeness $\Theta_{\text{max}} = 98.2\%$, 4852 independent reflections, $R_{\text{int}} = 0.026$, 3741 reflections with $F_o > 4\sigma(F_o)$, 298 parameters, 0 restraints, $R_{\text{obs}}^1 = 0.045$, $wR_{\text{obs}}^2 = 0.119$, $R_{\text{all}}^1 = 0.064$, $wR_{\text{all}}^2 = 0.130$, GOOF = 1.038, largest difference peak and hole: 0.544/–0.510 e Å⁻³.

2.4.4. Crystal data for **Fe3–NO**

C₂₆H₂₆FeN₅O₅, $M_r = 544.37$ g mol⁻¹, brown prism, size 0.19 × 0.17 × 0.12 mm, orthorhombic, space group $Pbncn$, $a = 38.8930(10)$, $b = 8.1527(3)$, $c = 15.2520(6)$ Å; $T = -90$ °C, $Z = 8$, $\rho_{\text{calc}} = 1.495$ g cm⁻³, μ (Mo Kα) = 6.73 cm⁻¹, $F(000) = 2264$, 9424 reflections in $h(-50/50)$, $k(-9/9)$, $l(-19/19)$, measured in the range

$2.88 \leq \theta \leq 27.51^\circ$, completeness $\theta_{\max} = 95.4\%$, 5303 independent reflections, $R_{\text{int}} = 0.095$, 3180 reflections with $F_o > 4\sigma(F_o)$, 334 parameters, 0 restraints, $R_{\text{obs}}^1 = 0.069$, $wR_{\text{obs}}^2 = 0.119$, $R_{\text{all}}^1 = 0.138$, $wR_{\text{all}}^2 = 0.138$, GOOF = 1.007, largest difference peak and hole: $0.447/-0.392 \text{ e } \text{Å}^{-3}$.

2.4.5. Crystal data for **Fe4–NO** × **MeOH**

$\text{C}_{23}\text{H}_{30}\text{FeN}_3\text{O}_{10}$, $M_r = 564.34 \text{ g mol}^{-1}$, brown prism, size $0.20 \times 0.18 \times 0.12 \text{ mm}$, monoclinic, space group $P2_1/n$, $a = 8.1399(2)$, $b = 11.5547(6)$, $c = 27.398(1) \text{ Å}$; $\beta = 96.018(3)^\circ$, $V = 2562.69(17) \text{ Å}^3$, $T = -90^\circ \text{C}$, $Z = 4$, $\rho_{\text{calc}} = 1.460 \text{ g cm}^{-3}$, $\mu (\text{Mo K}\alpha) = 6.49 \text{ cm}^{-1}$, $F(000) = 1176$, 9520 reflections in $h(-8/8)$, $k(-15/14)$, $l(-35/35)$, measured in the range $3.47 \leq \theta \leq 27.50^\circ$, completeness $\theta_{\max} = 89.7\%$, 5282 independent reflections, $R_{\text{int}} = 0.142$, 2348 reflections with $F_o > 4\sigma(F_o)$, 338 parameters, 0 restraints, $R_{\text{obs}}^1 = 0.079$, $wR_{\text{obs}}^2 = 0.158$, $R_{\text{all}}^1 = 0.210$, $wR_{\text{all}}^2 = 0.200$, GOOF = 0.997, largest difference peak and hole: $0.389/-0.501 \text{ e } \text{Å}^{-3}$.

2.4.6. Crystal data for **Fe5–NO** × **MeOH(1)**

$\text{C}_{19}\text{H}_{20}\text{FeN}_5\text{O}_6$, $M_r = 470.25 \text{ g mol}^{-1}$, dark-brown prism, size $0.28 \times 0.22 \times 0.20 \text{ mm}$, monoclinic, space group $P2_1/n$, $a = 7.4269(8)$, $b = 14.625(2)$, $c = 19.927(2) \text{ Å}$; $\beta = 91.790(8)^\circ$, $V = 2163.4(4) \text{ Å}^3$, $T = -90^\circ \text{C}$, $Z = 4$, $\rho_{\text{calc}} = 1.444 \text{ g cm}^{-3}$, $\mu (\text{Mo K}\alpha) = 7.42 \text{ cm}^{-1}$, $F(000) = 972$, 5056 reflections in $h(-9/9)$, $k(-18/0)$, $l(-25/0)$, measured in the range $2.47 \leq \theta \leq 27.45^\circ$, completeness $\theta_{\max} = 99.7\%$, 4922 independent reflections, $R_{\text{int}} = 0.038$, 2795 reflections with $F_o > 4\sigma(F_o)$, 360 parameters, 0 restraints, $R_{\text{obs}}^1 = 0.041$, $wR_{\text{obs}}^2 = 0.097$, $R_{\text{all}}^1 = 0.131$, $wR_{\text{all}}^2 = 0.122$, GOOF = 0.979, largest difference peak and hole: $0.405/-0.345 \text{ e } \text{Å}^{-3}$.

2.4.7. Crystal data for **Fe5–NO** × **MeOH(2)**

$\text{C}_{19}\text{H}_{20}\text{FeN}_5\text{O}_6$, $M_r = 470.25 \text{ g mol}^{-1}$, brown prism, size $0.12 \times 0.10 \times 0.09 \text{ mm}$, triclinic, space group $P\bar{1}$, $a = 8.574(1)$, $b = 8.955(1)$, $c = 15.638(1) \text{ Å}$; $\alpha = 86.804(7)^\circ$, $\beta = 76.623(6)^\circ$, $\gamma = 64.604(5)^\circ$; $V = 1053.9(2) \text{ Å}^3$, $T = -90^\circ \text{C}$, $Z = 2$, $\rho_{\text{calc}} = 1.475 \text{ g cm}^{-3}$, $\mu (\text{Mo K}\alpha) = 7.63 \text{ cm}^{-1}$, $F(000) = 480$, 7324 reflections in $h(-11/10)$, $k(-11/11)$, $l(-19/18)$, measured in the range $3.28 \leq \theta \leq 27.75^\circ$, completeness $\theta_{\max} = 93.7\%$, 4658 independent reflections, $R_{\text{int}} = 0.084$, 3153 reflections with $F_o > 4\sigma(F_o)$, 280 parameters, 0 restraints, $R_{\text{obs}}^1 = 0.167$, $wR_{\text{obs}}^2 = 0.204$, $R_{\text{all}}^1 = 0.226$, $wR_{\text{all}}^2 = 0.226$, GOOF = 1.214, largest difference peak and hole: $0.641/-0.558 \text{ e } \text{Å}^{-3}$.

2.4.8. Crystal data for **Fe6–NO**

$\text{C}_{18}\text{H}_{18}\text{FeN}_3\text{O}_5$, $M_r = 412.20 \text{ g mol}^{-1}$, brown prism, size $0.22 \times 0.18 \times 0.10 \text{ mm}$, monoclinic, space group $P2_1/n$, $a = 5.4089(4)$, $b = 16.108(1)$, $c = 20.205(1) \text{ Å}$; $\beta = 93.995(4)^\circ$, $V = 1756.1(2) \text{ Å}^3$, $T = -90^\circ \text{C}$, $Z = 4$, $\rho_{\text{calc}} = 1.559 \text{ g cm}^{-3}$, $\mu (\text{Mo K}\alpha) = 8.95 \text{ cm}^{-1}$,

$F(000) = 852$, 6433 reflections in $h(-6/6)$, $k(-18/20)$, $l(-25/25)$, measured in the range $3.29 \leq \theta \leq 27.32^\circ$, completeness $\theta_{\max} = 98.1\%$, 3869 independent reflections.

3. Results and discussion

3.1. Syntheses, general characterisation and reactivity

The iron(II) complexes **Fe1–Fe7** (with exception of **Fe7b**) and several of their iron(III) derivatives have been described earlier [12,13,16]. Their properties reflect the strong effect of the equatorial ligand and—if present—of additional axial ligands.

The macrocyclic complexes **Fe1–Fe3** having the strongest equatorial ligands exist mainly either as penta (4+1) coordinated species with intermediate spin ground state ($\text{Fe}^{\text{II}}: S = 1$; $\text{Fe}^{\text{III}}: S = 3/2$) or as octahedral derivatives with low spin ground state ($S = 0, 1/2$) [12,13,16]. Their first oxidation potentials are always metal centred ($\text{Fe}^{\text{II/III}}$) and can serve as a measure of the electron density at the central atom. They are strongly dependent on the macrocyclic ligand, the solvent and on the type of additional axial ligands. For **Fe1** (with $\text{R}^2 = \text{COMe}$ instead of COOEt) in MeCN a spread over more than 0.7 V has been observed [16e] (for better comparability all the following selected values are estimated for NHE by $E_{\text{H}}(\text{Fe}^{\text{II/III}}) = E_{\text{ref}}(\text{Fe}^{\text{II/III}}) + E_{\text{H}}(\text{ref})$ using $E_{\text{H}}(\text{Ag}^+) = -0.163 \text{ V}$ in MeCN and $E_{\text{H}}(\text{SCE}) = 0.241 \text{ V}$, tNC: tosylmethylisocyanide; chNC: cyclohexylisocyanide):

Axial ligand	tNC	MeCN	chNC
$E_{\text{H}}(\text{Fe}^{\text{II/III}})/\text{V}$	0.17	0.05	0.02
4CNPy	Py	N-MeIm	CN^\ominus
−0.02	−0.16	−0.39	−0.56

Depending on the macrocyclic ligand the potentials increase under identical conditions with decreasing electron density in the order

Electron density	Fe1	Fe2	Fe3
$E_{\text{H}}(\text{MeCN})/\text{V}$ [12b,16e]	0.05	0.34	0.69
$E_{\text{H}}(\text{Py})/\text{V}$ [16e]	−0.16	0.02	0.15

(As expected, the *trans*-axial binding of the donor pyridine becomes stronger with increasing Lewis acidity of the central atom and levels the electron density. This results in a lower gradation of the potentials.)

The complexes **Fe4–Fe7** with the two (more electro-negative) oxygen donors in the (weaker) open-chain ligand give mainly high spin derivatives ($\text{Fe}^{\text{II}}: S = 4/2$, $\text{Fe}^{\text{III}}: S = 5/2$) in a square pyramidal pentacoordinated (e.g. **Fe^{II}6a** × **HIm** [13,27], **Fe^{III}L** × **halide** [13,16a]) or

octahedral coordination sphere [13]. Exceptions were found with strong axial ligands such as imidazole (the low spin $S=0$ derivative **Fe6a** \times **2HIm** undergoes a transition into the high spin $S=4/2$ state above 328 K [13,27,28]). The adduct **Fe^{II}6a** \times **2Py** is high spin at r.t. but changes to low spin below 180 K [13,27]. The oxidation potentials in pyridine are—as expected—more positive than those of the macrocycles. They indicate clearly the increasing electron-withdrawing influence of the peripheral substituents on the electron density in the order ($E_H = E_{SCE} + 0.24$ V):

	Fe7b >	Fe6 >	Fe6a >	Fe7a >	Fe4 >	Fe5
$E_H(\text{Py})/\text{V}$	≈ 0.34	0.38	0.42	0.44	0.46	> 0.6
$E_H(\text{DMF})/\text{V}$	≈ 0.27	0.25	0.25	0.38	0.27	0.41

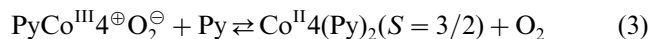
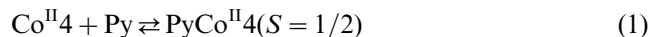
(DMF seems to be a stronger donor than pyridine in this case and lowers the potentials. Additionally, its high tendency to form H-bridges with the ligand periphery results in a more complicated dependence [16a].)

The differences of the oxidation potentials are manifested in the air sensitivity of the iron(II) complexes: The macrocycles—especially **Fe1**—are extremely sensitive to oxygen, independent of the axial ligands. The open-chain complexes vary in their air sensitivity from stable as solid over years (**Fe5** \times **3Py**) or for a few days (**Fe4** \times **2Py**) to highly air sensitive (ethylene bridged open-chain complexes).

This different sensitivity to air is also reflected in the reaction with nitric oxide. The macrocyclic complexes react in solution (e.g. methanol) very fast with NO undergoing a colour change from dark red or violet to dark green or brown–green. The nitrosyl derivatives (fine crystalline black solids) can be stored as solids at air for a few days without decomposition. The open-chain complexes **Fe6** and **Fe7a,b** behave similarly. The complex **Fe7b-NO** is the only ethylene bridged open-chain iron nitrosyl complex where a defined, pure product could be obtained.

The reaction of **Fe4** and **Fe5** requires a higher partial pressure of NO for complete transformation. As crystalline solids the open-chain nitrosyl complexes can be exposed to air for a few min, but longer exposition results in decomposition. The complexes **Fe4-NO** \times **MeOH** and **Fe5-NO** \times **MeOH** must be stored at temperatures below r.t. (freezer) to prevent a loss of methanol. The formation of the solvent free derivatives can be followed by IR spectroscopy (shift of the NO-stretching frequency to higher frequencies). These nitrosyl complexes decompose under argon in pure solvents (without excess of NO) to give the iron(II) complex and free nitric oxide. The elimination of NO (indicated in form of gas bubbles) is accelerated by addition of pyridine to a solution of the complexes in methanol or toluene. The iron(II) complexes crystallise as their adducts with pyridine, the starting materials for the synthesis of the nitrosyl derivatives. This reversible

reaction with NO, depending on the concentration of an potential axial ligand, resembles the equilibrium reaction of the corresponding cobalt(II) complex with dioxygen in presence of different concentrations of pyridine [13,15a], e.g.



A slower decomposition, accelerated by coordinating solvents or potential axial bases, was observed also for **Fe7b-NO**.

The nitrosyl derivatives of **Fe6a,b** are better soluble and require a much longer time for crystallisation. This may be the reason for difficulties in isolation of pure products. **Fe6a-NO** always contains small impurities of the μ -oxo derivative (**Fe6a**)₂O, and we could not isolate **Fe6b** in satisfactory purity.

Table 2
Selected IR data of the iron complexes with different axial ligands

Complex	ν_{NO} (cm^{-1})	ν_{CO} or ν_{CN} (cm^{-1})
Fe1		1671
Fe1-Cl		1680
Fe1-NO	1629	1678
Fe2		1676
Fe2-Cl		1685
Fe2-NO	1637	1676
Fe3		1686
Fe3-Cl		1697, 1683
Fe3-NO	1675	1700, 1687
Fe4 \times 2MeOH		1669
Fe4 \times 2Pyridin		1687 (1697 ^a)
Fe4-Cl		1693
Fe4-NO \times MeOH	1716	1698
Fe5		2220 (CN) ^a
Fe5 \times 3Pyridin		2201; 2184 (CN)
(Fe5) ₂ O		2207 (CN)
Fe5-NO	1776 ^b /1812	2200, 2204 (CN)
Fe5-NO ^c MeOH(1)	1744	2204, 2152 (CN)
Fe6		1655 ^a
Fe6 \times 2MeOH		1619
Fe6-Cl		1662
Fe6-NO	1790 (s), 1717 (w)	1638
Fe6a		1715 ^a
Fe6a-NO	1776	1704
Fe7a \times 2Py		1671 (1685 ^a)
Fe7a-NO	1778	1677
Fe7b \times 2Py		1671 (1605, 1598. ...)
Fe7b-NO		1700, 1696, 1659, 1655? ^d

^a These earlier in KBr measured values [16a] are about 10 cm^{-1} higher than those performed in nujol mull with the new instrumentation.

^b This band shows time-dependent increasing intensity and is apparently to assign to an impurity of a more stable octahedral isomer with intermolecular CN-coordination.

^c R.t. modification.

^d Doubtless assignment to the ν_{NO} difficult.

All the fine crystalline black precipitates are characterised by a new IR band which is with exception of **Fe7b-NO** well separated from the CO or CN stretching frequency of R^2 (Table 2). The $\nu(\text{NO})$ stretching frequencies of the derivatives without additional axial ligands increase from 1629 cm^{-1} for **Fe1-NO** to 1812 cm^{-1} for **Fe5-NO** and show a significant correlation with the increasing oxidation potentials of the iron(II) complexes. This suggests—with respect to the stretching frequency $\nu(\text{NO}^{\cdot}) = 1906.5\text{ cm}^{-1}$ for the $^2\Pi$ state of the free NO radical—an increasing population of the anti-bonding π^* orbital [29] with increasing electron density at the central atom. As expected, an additional trans donor ligand (MeOH in the adducts of **Fe4-NO** \times MeOH and **Fe5-NO** \times MeOH) increases the charge transfer to the NO ligand and lowers the NO frequency. The NO derivatives of our complexes which belong to the $\{\text{FeNO}\}^7$ type in the Enemark–Feltham notation [8]

could therefore be interpreted as $d^5 [\text{Fe}^{\text{III}}\text{L}^{\oplus}\text{NO}^{\ominus}]$ species—at least those of the macrocycles. Their $\nu(\text{NO})$ frequencies are within the range of $1520\text{--}1720\text{ cm}^{-1}$ which is considered for anionic NO^{\ominus} in its complexes, but for NO as three electron donor (bound as NO^{\oplus}) a similar broad range ($1950\text{--}1600\text{ cm}^{-1}$) is discussed, too [31]. The formulation Fe^{III} and NO^{\ominus} was also elucidated by Solomon et al. [30] on the base of detailed experimental and theoretical studies for other nitrosyliron complexes.

The formation of the NO derivatives from the iron(II) complexes is accompanied by a typical change of the Vis absorption spectrum. This is displayed in Fig. 1 for **Fe1**. The NO derivative is characterised by a new broad band at about 615 nm. It resembles the typical visible CT-absorption of pentacoordinated iron(III) derivatives **Fe1-X** (X: halide, N_3^- , NCS^-) [12c,13], but the intensity is much lower, and its wavelength is hardly

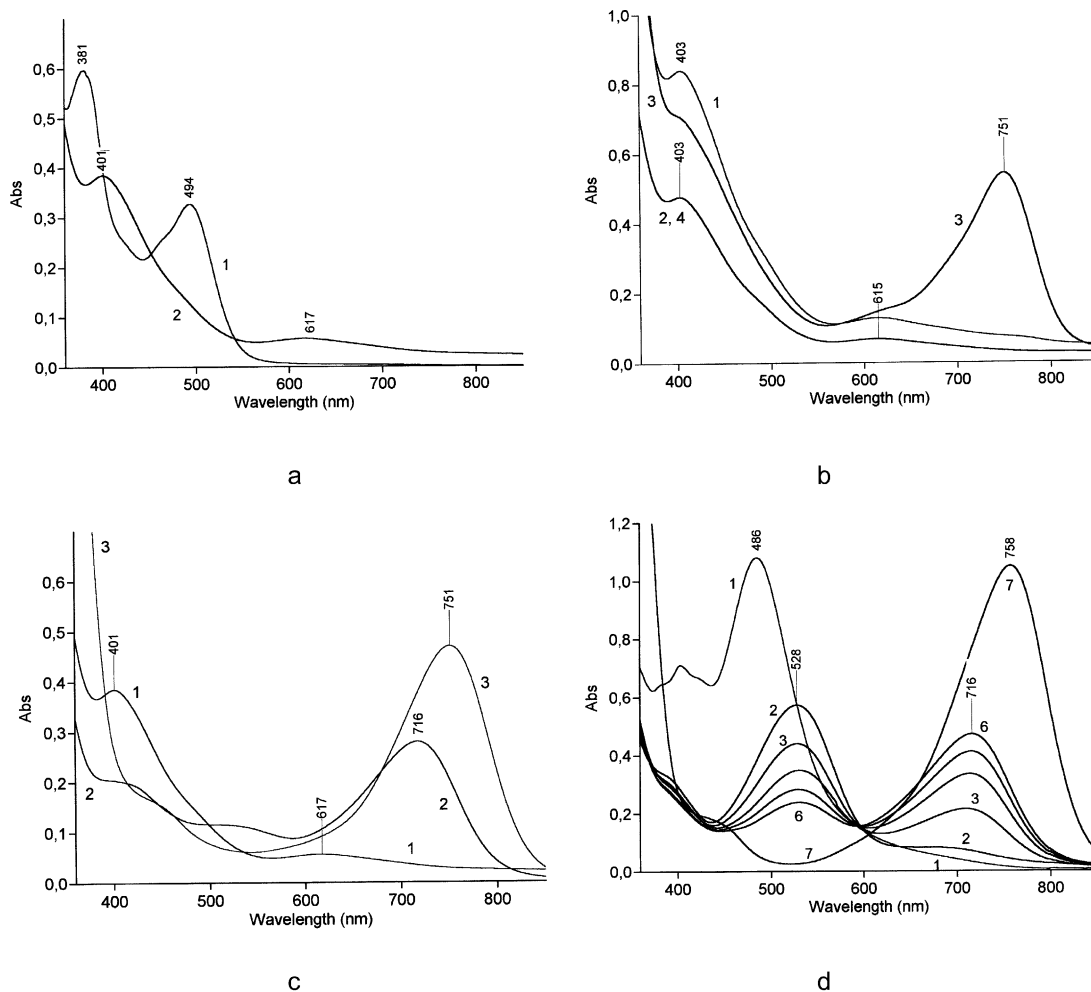


Fig. 1. Vis-Spectra of Fe-1 and their derivatives (a) $[\text{Fe}^{\text{II}}]$ (1) and $[\text{Fe}^{\text{I}}\text{-NO}]$ (2) in MeOH (inert). (b) $[\text{Fe}^{\text{I}}\text{-NO}]$ in toluene (2 = 4; $c = 0.0011\text{ M}$) and pyridine (1, 3; $c = 0.0022\text{ M}$) inert (1, 2) and after exposure to air (3, 4; the band at 751 nm increases strongly, and the shoulder at 403 nm decreases after longer interaction with air). (c) $[\text{Fe}^{\text{III}}\text{1-NO}_2 \times \text{MeOH}]$ (2) and $[\text{Fe}^{\text{III}}\text{1}(\text{NO}_2)_2]^-$ (3) formed from $[\text{Fe}^{\text{I}}\text{-NO}]$ in MeOH (1) by oxidation with air (2) followed by addition of NaNO_2 (3). (d) $[\text{Fe}^{\text{III}}\text{1-Cl}]$ in CH_2Cl_2 (1); $[\text{Fe}^{\text{III}}\text{1}_{\text{solv}}]^+$ from $[\text{Fe}^{\text{III}}\text{1-Cl}]$ in MeOH (2); 'titration' with an equimolar solution of $[\text{Fe}^{\text{III}}\text{1}(\text{NO}_2)_2]^-$ in MeOH (3–6) and saturated with NaNO_2 (7).

Table 3
UV–Vis data of FeI–NO^a

Solvent	<i>c</i> (mol l ⁻¹)	λ_1 (nm)	Log (ϵ_1 /(l mol ⁻¹ cm ⁻¹))	λ_2 (nm)	Log (ϵ_2 /(l mol ⁻¹ cm ⁻¹))
Methanol	7.4×10^{-4}	401	3.72	616	2.88
Toluene	1.1×10^{-3}	403	3.64	614	2.78
Pyridine	2.2×10^{-3}	405	3.58	614	2.76

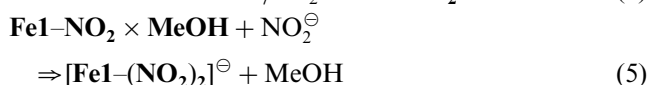
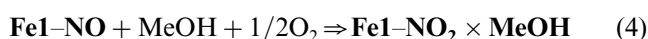
^a All spectra were measured at r.t. under argon with *d* = 0.1 cm.Table 4
Potentials and kinetic data for the electrochemical reduction^a of selected nitrosyliron complexes in methylenechloride+0.5 m Bu₄NClO₄

Complex (type)	$E_{Ag^{\circ}}$ (V)	k_s (cm s ⁻¹)	<i>D</i> (cm ² s ⁻¹)
FeI–NO (I)	-0.775(-1.01)	0.3	8×10^{-6}
Fe2–NO (I)	-0.660(-0.90)	0.8	8×10^{-6}
Fe3–NO (I)	-0.520(-0.76)	1.0	7×10^{-6}
Fe7b–NO (II)	-0.410(-0.65)	0.3	5×10^{-6}
		E_{pc} (V) ^b	E_{pa} (V)
Fe6–NO (II)	-0.345(-0.58)	-0.375	-0.314...-0.317 ^{c,d}
Fe6a–NO (II)	-0.345(-0.58)	-0.375	-0.313
Fe5–NO (II)	-0.133...-0.128 ^c (-0.37)	-0.158...-0.155 ^c	-0.107...-0.101 ^c

^a Hanging mercury drop; vs. Ag–AgCl–MeCN+0.25 mⁿBu₄NCl. In parentheses: $E_H = E_{Ag^{\circ}} - 0.237$ V (see Section 2.3).^b Kinetic parameters not determined.^c With increasing scan-rate.^d Weak satellite at lower potential, caused probably by partial isomerisation; not observed in MeCN.

dependent on the solvent (Table 3). This independence of the spectrum under anaerobe conditions indicates that the pentacoordinated complex does not bind an additional axial ligand (MeOH, pyridine). Indeed, our attempts to obtain any adducts of the macrocyclic complexes FeI–NO to Fe3–NO were not successful. Recrystallisation from MeOH–Py yields the pure solvent free starting material. In contrast, some of the complexes with open-chain ligands were isolated from methanol as their monoadducts FeL–NO × MeOH.

As solids and as solutions in non-coordinating solvents (toluene) FeI–NO, Fe2–NO and Fe3–NO are stable on air for some time without decomposition. In coordinating solvents (pyridine; MeOH) the reaction with dioxygen is indicated by a characteristic change of the spectrum (displayed for FeI–NO in pyridine in Fig. 1(b), curve 3). A detailed spectral comparison of the products formed by oxidation of FeI–NO in pyridine or MeOH, followed by addition of sodium nitrite (Fig. 1(c)), with those formed from Fe^{III}I–I or Fe^{III}I–Cl in MeOH (Fig. 1(d)) or pyridine by titration with sodium nitrite, reveal without any doubt the following sequence for the observed reactions:



The stability of the intermediate FeI–NO₂ × MeOH

over a broad range of nitrite concentration is in agreement with the observation, that nitro derivatives of our macrocyclic iron(III) complexes were often isolated with an *trans*-axially bound O-donor, e.g. Fe2–NO₂ × H₂O [13,32].

The complexes Fe4–NO × MeOH, Fe5–NO × MeOH, and Fe5–NO are air sensitive even in non-coordinating solvents. The aerobic decomposition results in the formation of the corresponding μ-oxo-species as the main product.

Table 5
Oxidation potentials of macrocyclic nitrosyliron complexes measured by cyclic voltammetry (CV) and square wave voltammetry (SWV)

Complex	ΔE_p (mV)	$E_{Ag^{\circ}}$ (V) (CV)	$E_{Ag^{\circ}}$ (V) (SWV)	E_{fc} (V) ^d
FeI–NO ^a	68	0.975(0.74)	0.977...0.983 ^c	0.12
Fe2–NO ^a	72	0.815(0.58)	0.808...0.813 ^c	-0.04
Fe3–NO ^a	61	0.840(0.60)	0.834...0.841 ^c	-0.02
FeI–NO ^b	66	0.89 (0.73)		0.11
	76	1.16 (1.00)		0.38

^a In CH₂Cl₂+0.5 mⁿBu₄NClO₄; Pt disc electrode; vs. Ag–AgCl–MeCN+0.25 mⁿBu₄NCl. In parentheses: $E_H = E_{Ag^{\circ}} - 0.237$ V.^b In MeCN+0.5 mⁿBu₄NClO₄; Pt disc electrode; vs. Ag–AgCl–MeCN+0.25 mⁿBu₄NCl. In parentheses: $E_H = E_{Ag^{\circ}} - 0.163$ V.^c Shift with increasing frequency (six steps from 25 to 800 Hz).^d fc = ferrocen–ferricinium; $E_{Ag^{\circ}}$ (fc–fc⁺) = 0.857 V in methylenechloride, 0.785 V in MeCN.

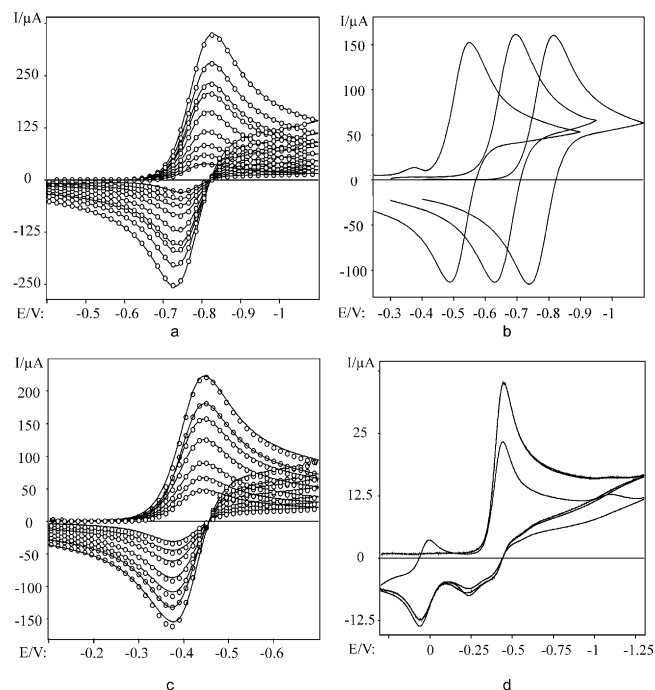


Fig. 2. Cyclic voltammetric reduction of selected complexes **I** and **II** (a) Comparison of experimental (solid line) and simulated (open circles) CVs for the reduction of **[Fe1-NO]** in CH_2Cl_2 (0.5 M $\text{nBu}_4\text{NClO}_4$, mercury drop electrode) at scan rates 2, 5, 10, 20, 40, 67, 83, 125 and 200 V s^{-1} , respectively. (b) Reduction of **[Fe3-NO]** (left), **[Fe2-NO]** (middle) and **[Fe1-2NO]** (right) in CH_2Cl_2 (0.5 M $\text{nBu}_4\text{NClO}_4$, mercury drop electrode) at a scan rates of 40 V s^{-1} . (c) Comparison of experimental (solid line) and simulated (open circles) CVs for the reduction of **[Fe7b-NO]** in CH_2Cl_2 (0.5 M $\text{nBu}_4\text{NClO}_4$, mercury drop electrode) at scan rates 5, 10, 20, 40, 62, 83 and 125 V s^{-1} , respectively. (d) First and second cycle of the cyclic voltammetric reduction of **[Fe7b-NO]** in CH_2Cl_2 (0.5 M $\text{nBu}_4\text{NClO}_4$, mercury drop electrode) at a scan rates of 1 V s^{-1} .

From **Fe5-NO** \times **MeOH** two isomers were isolated depending on the temperature of preparation (cf. Section 2.4.6 and Section 2.4.7). Both show significant differences in stability and molecule structure. The low-temperature isomer **Fe5-NO** \times **MeOH(2)** converts quickly into the stable isomer **Fe5-NO** \times **MeOH(1)** at r.t. Therefore, we were not able to measure the characteristic spectroscopic, electrochemical and magnetic data for the low temperature form. Fortunately it was possible, however, to solve the crystal and molecule structure of both isomers by X-ray analysis (cf. Section 3.4).

3.2. Electrochemistry

The redox behaviour of the new nitrosyliron complexes was investigated using cyclovoltammetry (and, in part, frequency dependent square wave voltammetry) in

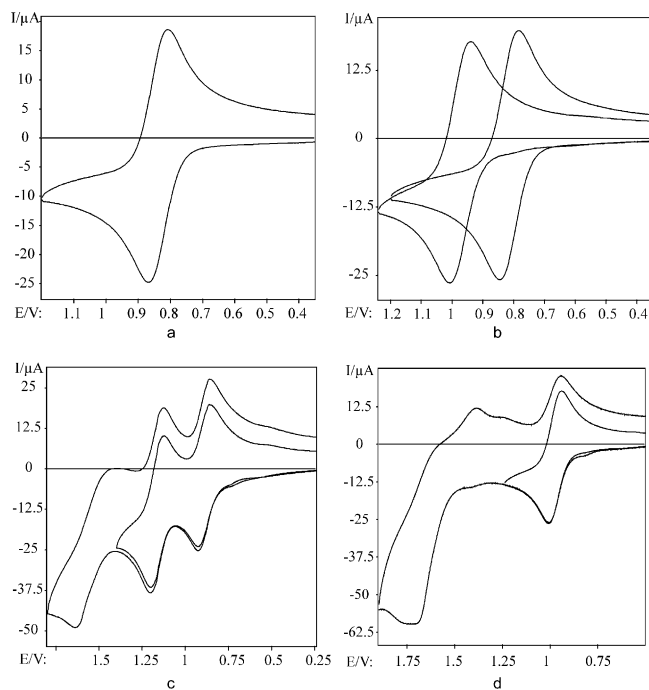


Fig. 3. Voltammetric oxidation of selected complexes **I** and **II** (a) Oxidation of **[Fe3-NO]** in CH_2Cl_2 (0.5 M $\text{nBu}_4\text{NClO}_4$, Pt-disk electrode) at a scan rate of 1 V s^{-1} . (b) Cyclic voltammetric oxidation of **[Fe1-NO]** (left) and **[Fe2-NO]** (right) in CH_2Cl_2 (0.5 M $\text{nBu}_4\text{NClO}_4$, Pt-disk electrode) at a scan rate of 1 V s^{-1} . (c) Cyclic voltammetric oxidation of **[Fe1-NO]** in acetonitrile (0.5 M $\text{nBu}_4\text{NClO}_4$, Pt-disk electrode) at a scan rate of 1 V s^{-1} . (d) Cyclic voltammetric oxidation of **[Fe1-NO]** in CH_2Cl_2 (0.5 M $\text{nBu}_4\text{NClO}_4$, Pt-disk electrode) at a scan rate of 1 V s^{-1} .

methylenechloride, for **Fe1-NO** also in MeCN. The results are listed in Tables 4 and 5. Characteristic examples of voltammograms are displayed in Figs. 2–4.

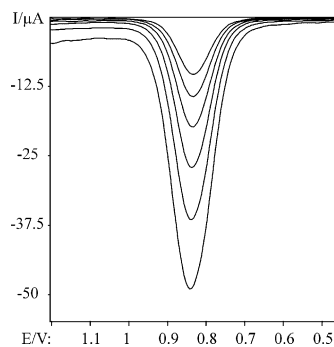


Fig. 4. Square wave voltammograms of the oxidation of **[Fe3-NO]** in CH_2Cl_2 (0.5 M $\text{nBu}_4\text{NClO}_4$, Pt-disk electrode) at frequencies of 25, 50, 100, 200, 400 and 800 s^{-1} (order of increasing peak currents) using a square wave amplitude of 25 mV and potential steps of 5 mV. The SW voltammograms show a small frequency-dependent potential shift of 6 mV indicating a slow follow-up reaction of the oxidised species, which cannot be detected in the CVs depicted in Fig. 3(a).

Fig. 5. Temperature dependence of the effective magnetic moment of selected nitrosyl derivatives of iron complexes with macrocyclic Fe1NO and open-chain ligands type II. All measurements were carried out at two magnetic field strengths, e.g. 0.2 and 0.5 T. The deviations are within the circles in the curves as displayed for **Fe5NO** and **Fe7b NO**.

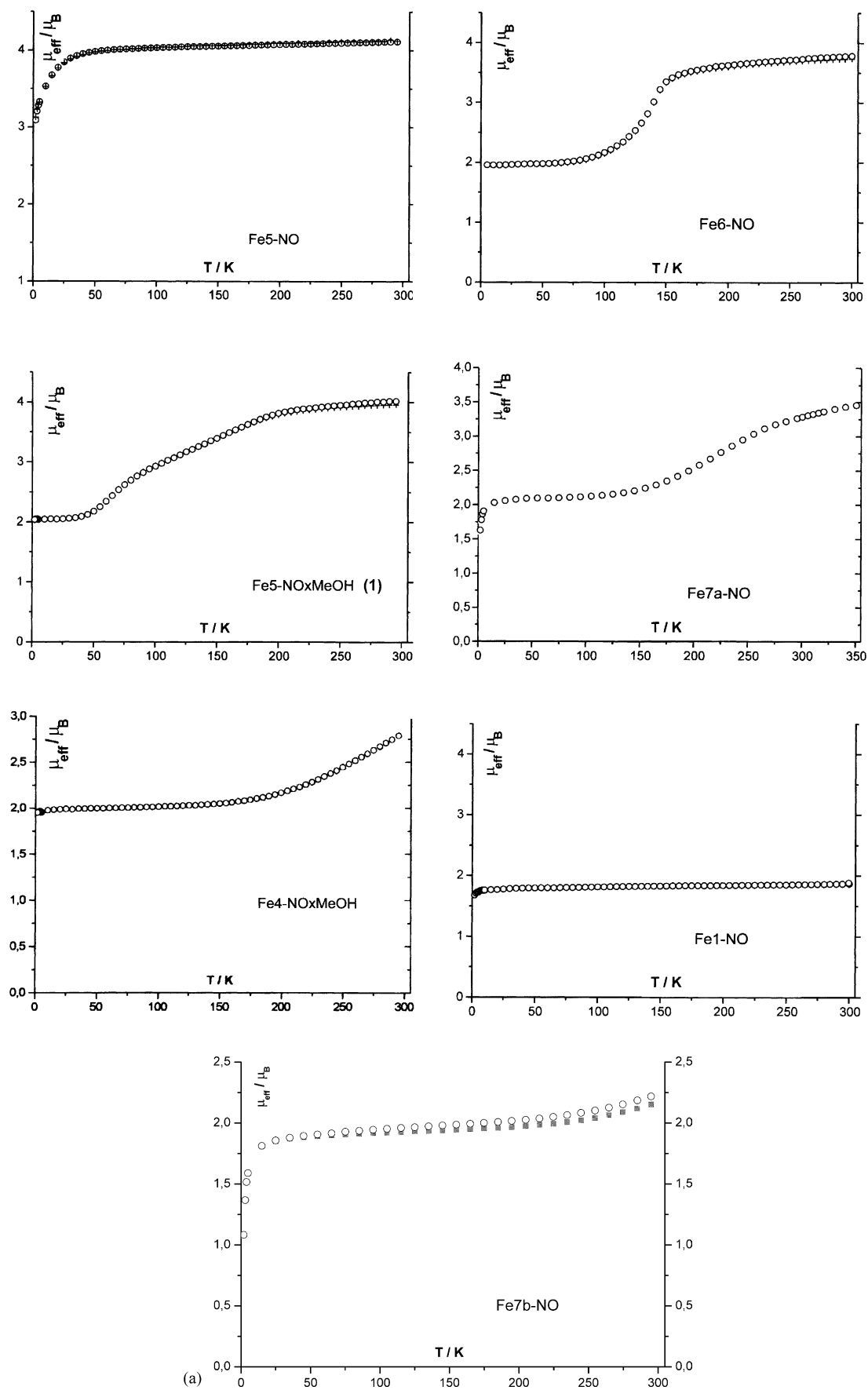


Fig. 5

All nitrosyl complexes show a (quasi)reversible reduction (Table 4). In case of the macrocycles **Fe1–NO** to **Fe3–NO** and the aliphatically bridged open-chain complex **Fe7b–NO** the kinetic parameter could be determined by simulation of the CVs using the Digi-SimTM algorithm [33,34] (cf. Table 4 and the examples of Fig. 2(a), (c)). Remarkable are the relatively high rate constants k_s for the heterogeneous electron transfer reaction. They are in the same magnitude as those observed for planar nickel complexes of type **I** [17] and **II** [35]. The values of the macrocyclic complexes increase with increasing extension of the π -electron system when aliphatic bridges are successively replaced by aromatic bridges.

The NO derivatives with open-chain ligands are less stable in solution without an excess of free NO. The lower affinity towards NO becomes particularly visible if the complex is reduced in a CV experiment. As shown in Fig. 2(d), the second cycle at the low scan rate of 1 V s^{-1} exhibits a decimated signal of the nitrosyliron redox couple and a new signal of the NO-free $\text{Fe}^{\text{II/III}}$ redox couple. **Fe5–NO** and **Fe6–NO** show a small but significant drift of the peak potentials in dependence on the scan rate (Table 4). Additionally, in some cases (e.g. **Fe6a–NO**) the CVs indicate small impurities of the μ -oxo iron(III) complex that is formed by oxidative decomposition of the nitrosyl derivatives. The CVs of **Fe6–NO** in methylenechloride (but not in MeCN) show a weaker satellite at lower potentials that is possibly caused by partial isomerisation of the complex in solution. (A similar peculiarity in solution had been observed in the EPR spectra of the pure cobalt(II) complex with the same ligand [36], although the crystal structure of **Co6** indicates only identical molecules in solid state.) No evaluable CVs were obtained with the complex **Fe4–NO**.

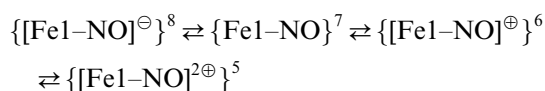
The values of the equilibrium reduction potentials of the nitrosyl derivatives show the same trend in dependence on the equatorial ligand (cf. Table 4, Fig. 2(b)) as the $\text{Fe}^{\text{II/III}}$ couples of the base iron(II) complexes (cf. Section 3.1), but on a much lower (more negative) level. The potentials are significantly (non-linear) correlated with the $\nu(\text{NO})$ stretching frequency. This behaviour suggests all in all the interpretation of the one electron reduction of the nitrosyl derivatives as a mainly metal centred $\text{Fe}^{\text{II/III}}$ couple. The low level of the potentials could be explained with the presence of anionic NO^- as a very strong axial donor ligand. The potential becomes more negative with increasing electron donating effect of the equatorial and the NO ligand (i.e. increasing electron density on the iron), and the $\nu(\text{NO})$ decreases because the transfer of electron density from the antibonding $\text{NO } \pi^*$ orbital to the central atom becomes more difficult.

The macrocycles give also a reversible couple $[\text{FeL–NO}]^0/[\text{FeL–NO}]^+$ for the one electron oxidation (Table

5, Fig. 3(a),(b)). The potentials measured by cyclic voltammetry and by square wave voltammetry (Fig. 4) are in good agreement, although the latter show a small but significant shift depending on the frequency. The gradation of the equilibrium potentials in dependence on the equatorial macrocycle is different from those found for the oxidation of the base iron(II) complexes and for the reduction of their nitrosyl derivatives. The complex **Fe1–NO** with the strongest electron-donating macrocycle shows the most positive potential (0.97 V vs. 'Ag'), whereas **Fe2–NO** and **Fe3–NO** have lower and scarcely different values (0.82 and 0.84 V, respectively). The base iron(II) complexes **Fe1**, **Fe2** and **Fe3**, show a second oxidation $[\text{FeL}]^{1+/2+}$ in methylenechloride at $E_{\text{Ag}^+} = 1.46, 1.30$ and 1.27 V , respectively, which had been classified as belonging to $\text{Fe}^{\text{III/IV}}$ for **Fe1** and to an oxidation of the aromatically bridged anionic macrocycle for **Fe2** and **Fe3** [12b]. The similar gradation of the oxidation potentials of the NO derivatives suggests an analogous interpretation, whereby the (*cis*-) influence of the strongly donating anionic NO^- ligand makes the (equatorial ligand-) oxidation easier and lowers the potential.

A quantity worth mentioning is the difference between the oxidation and the reduction potentials of the nitrosyl derivatives on the one hand (1.75, 1.48, and 1.33 V for **Fe1–NO** to **Fe3–NO**) and between the second and the first oxidation potentials of the base iron(II) complexes on the other hand (1.17, 0.75, and 0.71 V for **Fe1–Fe3**). It is a measure of the width of the thermodynamic stability of the middle oxidation state—in our imagination iron(III). This is in good agreement with the expectation in an electrostatic view: increasing electron-donating effect of the whole ligand sphere results in an increasing stabilisation of the iron(III) state.

The nitrosyl derivative **Fe1–NO** with the strongest equatorial donor ligand gives a second reversible oxidation (Fig. 3(c)), but only in MeCN ($E_{\text{Ag}^+} = 1.16 \text{ V}$) and not in methylenechloride (Fig. 3(d)). There is no counterpart of this in the redox chemistry of the base complex **Fe1**. Therefore, it should be assigned to a (MeCN-assisted?) mainly NO centred oxidation resulting in a $[\text{Fe}^{\text{IV}}\text{1–NO}^\bullet]^{2+}$ species. All in all, this complex with the aliphatically bridged equatorial $[\text{N}_4^{2-}]$ coordinated macrocycle is characterised by the following series of four reversible redox couples in the Enemark–Feltham notation:



The nitrosyl derivatives with equatorial open-chain ligands **Fe4–NO** to **Fe7–NO** give no reversible oxidation.

With respect to its reduction and oxidation potentials as well as their difference, the complex **Fe1-NO** is surprisingly closely related to the $\{\text{FeNO}\}^7$ species *trans*-[(cyclam)Fe(NO)Cl](ClO₄) (cyclam = 1,4,8,11-tetraazacyclotetradecane) that was synthesised and studied in detail (together with similar isostructural nitrosyl complexes) by Wieghardt, et al. [9]. This complex shows in MeCN reversible couples for the oxidation at 0.14 V and the reduction at -1.30 V (vs. *fc*-*fc*⁺). Based on variable-temperature Mössbauer spectroscopy in applied field, this complex with an *S* = 1/2 ground state was proposed to contain an intermediate spin (*S* = 3/2) iron(III) ion, antiferromagnetically coupled with an NO[⊖] anion in its triplet (*S* = 1) state. This interpretation—and for **Fe1-NO** also the description of the oxidation product as an iron(IV) complex—is in full agreement with our imagination of the NO binding mode in the macrocyclic complexes **Fe1-NO** to **Fe3-NO**. The product of the reduction, $\{[\text{FeL-NO}]^{\ominus}\}^8$, is in our case, however, rather an iron(II) species with an NO[⊖] monoanion than an iron(III) complex with an NO^{2⊖} dianion, as proposed for the above mentioned cyclam complex by Wieghardt et al. Attempts to isolate and characterise the reduction and oxidation products of our macrocyclic nitrosyl complexes are in progress.

3.3. Magnetochemistry

The magnetic susceptibilities of all new nitrosyliron complexes were measured from 1.7 to 300 K. In no case was a strict linear relationship between χ^{-1} and *T* according to the Curie–Weiss law observed. Apart from spin crossover processes within the investigated temperature range, there are in some cases (especially for **Fe7a-NO**, **Fe7b-NO**, in much weaker extent also for **Fe1-NO** to **Fe3-NO**) deviations at low temperature (< 10 K) which correspond with a decrease of the magnetic moment below the value for one unpaired electron. The reason for this—intermolecular antiferromagnetic coupling of a $\{\text{FeNO}\}^7$ complex or spin-orbit coupling in a NO[⊖] radical bound to low-spin Fe^{II}—is not clear. For better comparison of the ground state, the more informative magnetic moments μ_{eff} in dependence on the temperature are depicted for selected examples in Fig. 5.

All complexes with macrocyclic ligands have an *S* = 1/2 ground state over the whole temperature range—as it is displayed for **Fe1-NO** in Fig. 5. This is in agreement with the above mentioned interpretation as an intermediate spin (*S* = 3/2) iron(III), antiferromagnetically coupled with a coordinated NO[⊖] anion in its triplet (*S* = 1) state. This assumption is strongly supported by the fact, that all pentacoordinated iron(III) derivatives of our macrocycles, **FeL-X** (X = halide, pseudo halide), have also an *S* = 3/2 ground state—and a nearly identical geometry of the first coordination sphere (see

Table 6
Selected bond lengths (Å) and angles (°) for macrocyclic nitrosyliron complexes type I

Complex: bond/∠	Fe1-NO	Fe2-NO	Fe3-NO	FeMe ₄ - TAA-NO ^a
<i>Bond lengths</i>				
Fe–N1	1.928(2)	1.909(2)	1.914(3)	1.948
Fe–N2	1.895(2)	1.915(2)	1.935(3)	1.931
Fe–N3	1.920(2)	1.942(2)	1.975(3)	1.945
Fe–N4	1.954(2)	1.936(2)	1.945(3)	1.951
Fe–N(NO)	1.732(2)	1.712(2)	1.716(3)	1.716
Fe–pl(N ₄) _{eq} ^b	0.376	0.353	0.442	0.386
N–O	1.185(3)	1.164(3)	1.171(4)	1.165
<i>Bond angles</i>				
Fe–N–O	140.3(2)	145.1(2)	152.0(3)	144.0
N1–Fe–N2	83.46(10)	83.60(9)	82.19(12)	97.4
N3–Fe–N4	86.71(11)	86.11(10)	83.53(12)	83.1
N2–Fe–N3	91.51(11)	91.12(9)	91.74(13)	93.5
N4–Fe–N1	89.70(10)	91.57(9)	90.63(12)	92.4
N1–Fe–N–O ^c	+133.2	–15.9	+121.7	+117.8
Pl(N ₄) _{eq} –pl(FeNO) ^d	90.6	90.2	91.4	90.2
Tilt angle ^e	5.6	4.8	4.0	4.9

^a Data from CSD database v. 5.22 (Oct. 01) Code GEFNIO, cf. [7c].

^b Displacement of the iron from the equatorial [N₄] plane.

^c Torsion angle.

^d Dihedral angle between the equatorial [N₄] plane and the [FeNO] plane.

^e Tilt angle between the Fe–N(NO) bond and the axis vertical to the [N₄] plane.

below). The *S* = 1/2 state is also dominant in the complex **Fe7b-NO**, but the magnetic moment increases significantly above ≈ 250 K—indicating a slow transfer into a higher (*S* = 3/2?) spin state. This behaviour reflects the middle position of this aliphatically bridged complex between the macrocycles and the other (aromatically bridged) complexes with open-chain ligands (cf. the oxidation potential of the base iron(II) complexes, the reduction potential and the decomposition in solution of the nitrosyl derivatives etc.).

The pentacoordinated complex **Fe5-NO** with the most electron-withdrawing periphery of the equatorial ligand represents the other extreme: The magnetism corresponds with an *S* = 3/2 ground state which is stable down to about 30 K. An explanation for this should at least consider either a high spin iron(III) (*S* = 5/2), antiferromagnetically coupled with the triplet state of an NO[⊖] anion, or a high spin iron(II) (*S* = 2), antiferromagnetically coupled with the doublet (*S* = 1/2) state of a neutral NO[⊖] radical. Both possibilities would agree with the fact, that the base iron(II) complex **Fe5**—even with rather strong axial ligands—as well as its iron(III) derivatives are always high spin complexes (*S* = 4/2, 5/2). The first possibility was derived from combined physical measurements and spin polarised SCF-X α calculations by Solomon et al. [30] for Wieghardt's *S* = 3/2 nitrosyl complex Fe(Me₃-

Table 7
Selected bond lengths (Å) and -angles (°) for nitrosyliron complexes type **II** with open-chain $[\text{N}_2\text{O}_2]^{2-}$ ligands

Complex:	Fe4–NO × MeOH	Fe5–NO × MeOH(1) ^b	Fe5–NO × MeOH(2) ^c	Fe6–NO	FeSalen-NO(1) ^a	FeSalen-NO(2) ^a
<i>Bond lengths</i>						
Fe–N1	1.905(4)	2.015(2)	2.0728(16)	2.012	2.07(1)	1.97(2)
Fe–N2	1.915(4)	2.035(2)	2.0862(16)	1.966	2.08(1)	1.98(3)
Fe–O1	1.969(4)	2.014(2)	2.0601(14)	1.948	1.923(9)	1.93(2)
Fe–O2	1.977(4)	1.998(2)	2.0363(15)	1.956	1.892(9)	1.87(2)
Fe–O(MeOH)	2.252(4)	2.296(3)	2.2009(16)			
Fe–N(NO)	1.721(5)	1.761(3)	1.7796(18)	1.701	1.78(2)	1.793
Fe–pl($[\text{N}_2\text{O}_2]_{\text{eq}}$) ^d	0.175	0.237	0.177	0.504	0.465	0.360
N–O	1.169(6)	1.137(4)	1.107(3)	1.174	1.11(4)	1.15
<i>Bond angles</i>						
Fe–N–O	142.1(4)	149.5(3)	149.7(2)	167	144;150	122;132
N1–Fe–N2	83.97(19)	79.94(9)	78.69(6)	80.5	76.8	79.5
O1–Fe–O2	89.70(16)	96.71(10)	104.51(6)	90.5	95.1	88.9
N2–Fe–O1	92.32(17)	89.77(9)	87.41(6)	87.6	87.3	90.9
O2–Fe–N1	92.24(18)	90.41(10)	87.72(6)	86.5	88.1	92.7
N1–Fe–N–O ^e	+23.5	+14.7	–34.0	133.6	–34.6	–27.2
Pl _{eq} –pl(FeNO) ^f	90.3	90.7	93.1	89.0	87.3	90.8
Tilt angle ^g	4.4	4.5	3.8	2.8	2.9	5.3

^a Data from CSD database v. 5.22 (Oct. 01) Code NSALFE and NSALFE01, cf. [10].

^b Generated at r.t.

^c Generated at –68 °C.

^d Displacement of the iron from the equatorial $[\text{N}_2\text{O}_2]$ plane.

^e Torsion angle.

^f Dihedral angle between the equatorial $[\text{N}_2\text{O}_2]$ plane and the axial $[\text{FeNO}]$ plane.

^g Tilt angle between the Fe–N(NO) bond and the axis vertical to the $[\text{N}_2\text{O}_2]$ plane.

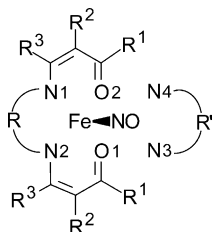


Fig. 6. Unified atom numbering scheme used in Tables 6–8 for the equatorial donor atoms. The numbers may deviate from those in Fig. 7.

TACN)(NO)(N_3)₂] (TACN = triazacyclononane) [37] and for the nitrosyl derivative of FeEDTA. For **Fe5–NO** the second possibility would be supported by the high oxidation potential of the base complex **Fe5**, the low reactivity of this iron(II) complex and the corresponding cobalt(II) complex **Co5** with dioxygen (which is in striking contrast to the behaviour of all the other iron(II) and cobalt(II) complexes studied in our laboratory [13,15a]), and by the low stability of **Fe5–NO** in solution (especially the relatively fast elimination of free NO in absence of an excess of NO and in presence of potential axial ligands). As the X-ray studies show (see

below), it seems that both possibilities are realised in the both isomers **Fe5–NO × MeOH(1)** and **Fe5–NO × MeOH(2)**.

The other complexes (including **Fe5–NO × MeOH(1)**) wherein the additional trans ligand increases the overall ligand field strength of **Fe5–NO** show the typical conversion between a low temperature $S = 1/2$ and a high temperature $S = 3/2$ state, that has been described earlier by König, Larkworthy et al. for **Fe6–NO** [7e,7f]. In respect to this, our 1,2-phenylene bridged complexes of the type **FeII–NO** are closely related to N,N' -ethylen-bis(salicylideneiminato)nitrosyliron, **Fe(salen)–NO**, which can be classified as belonging to the general type **II** with an annelated aromatic ring for $\text{R}^1 + \text{R}^2$. The latter was first described by Earnshaw, King and Larkworthy [38] to give an $S = 3/2 \Rightarrow S = 1/2$ transition at decreasing temperature—a phenomenon that was subsequently intensively studied by different experimental and theoretical methods [7d,7e,10]. In contrast to some of our type **II** complexes with $\text{R} = 1,2$ -phenylene, the corresponding nitrosyliron complexes of aromatically bridged salicylaldimines have in general a T -independent $S = 3/2$ ground state [38].

Fig. 7. Molecule structures of selected nitrosyliron complexes with macrocyclic N42 coordinated and open-chain N2O22 coordinated Schiff base ligands. All structures are displayed in approximately the same projection with NO as apex and the N1 of Fig. 6 in front left. FeMe4TAA is the complex Type I with RR1,2-phenylene, R1R3Me and R2H data taken from the CSD database 5.22, October 01, GEFNIO.

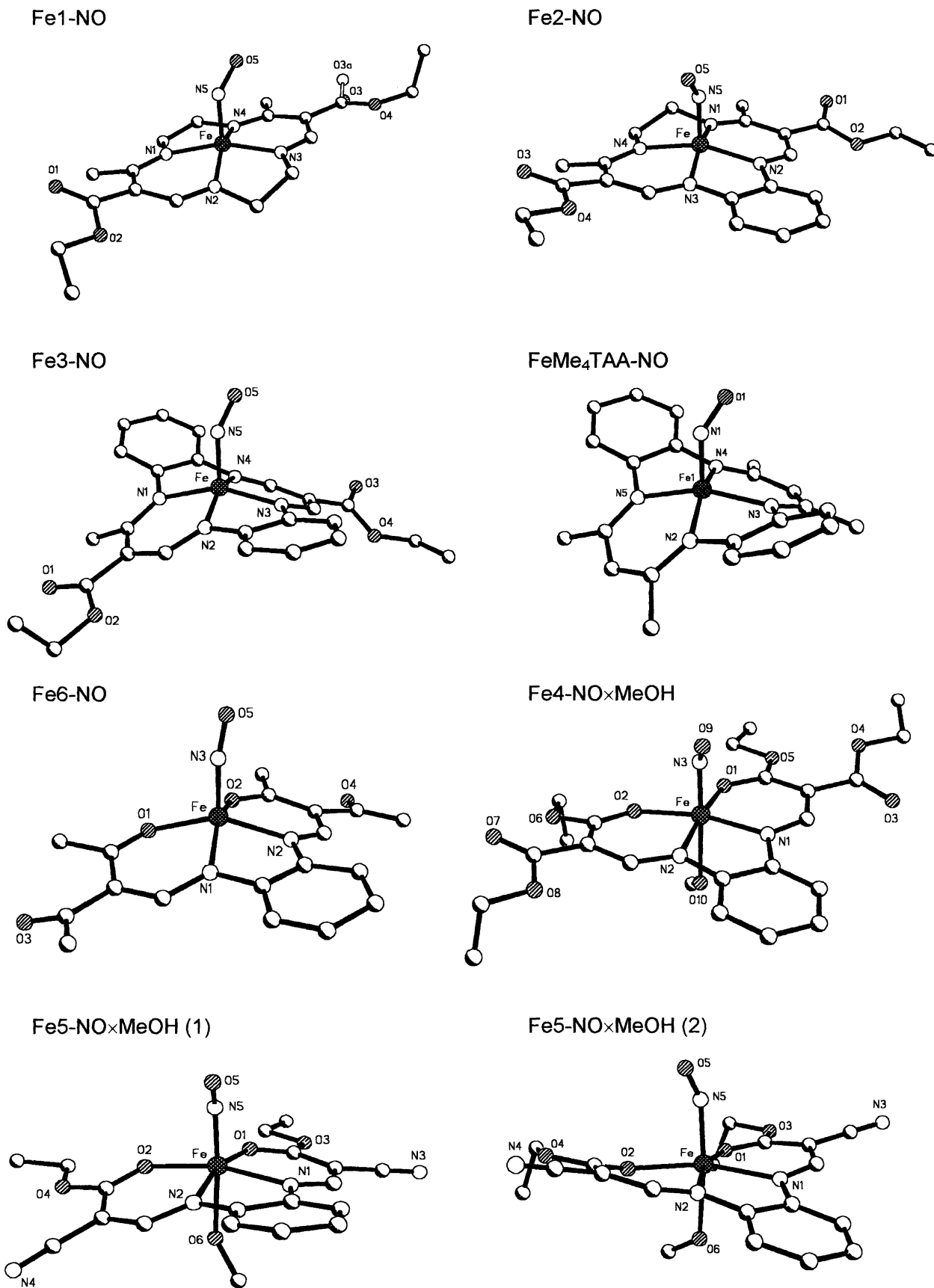


Fig. 7

It is interesting to note that some of the base iron(II) complexes of type **II** show similar spin crossover phenomena—depending on the number and strength of axial ligands. For instance, **Fe6a** gives a pentacoordinated mono adduct with imidazole, **Fe6a** × **HIm**, that is in the high spin ($S=2$) state, independent of the temperature. The corresponding diadduct, **Fe6a** × **2HIm**, is a low-spin ($S=0$) complex up to 325 K, where a very sharp and strictly reversible conversion into the high spin isomer takes place [13,27,28]. The octahedral adduct **Fe6a** × **2Py** with two pyridine (a weaker axial ligand than imidazole) undergoes a spin change between $S=0$ and $S=2$ at about 180 K [13]. Conversion between low spin ($S=1/2$) and high spin ($S=5/2$) states has also been observed for many iron(III) complexes with salen derivatives as equatorial chelate ligand [39].

Particular consideration ought to be paid to the spin conversion of the nitrosyliron complex **Fe5-NO** × **MeOH(1)**. It takes place in two badly separated but significant steps (Fig. 5). Such behaviour (spin transition ‘type d’ in the notation of Gütlich et al. [40]) is well established and intensively studied e.g. for $[\text{Fe}(\text{2-picolylamin})_3]\text{Cl}_2 \times \text{EtOH}$, and seems to be caused by a cooperative 1:1 ordering of low-spin and high spin molecules [40]. In our case, an intermolecular interaction through H-bridges between the MeOH ligand and the peripheral CN substituents could be responsible for such behaviour.

3.4. X-ray Investigations

Suitable crystals for X-ray structural investigations were obtained from all solvent free macrocycles **Fe1-NO**, **Fe2-NO** and **Fe3-NO**, the likewise solvent free **Fe6-NO**, as well as from the methanol monoadducts **Fe4-NO** × **MeOH** and **Fe5-NO** × **MeOH**—the latter in both preparations, the stable and the metastable isomer (1) and (2). Unfortunately, the attempts to isolate good crystals from the solvent free **Fe5-NO** and from the derivatives with $\text{R}^1 = \text{Ph}$, **Fe7a,b-NO**, failed. All measurements were carried out at -90°C . Under these conditions, the macrocycles are in the pure $S=1/2$ state whereas **Fe6-NO** and **Fe5-NO** × **MeOH(1)** should remain in the $S=3/2$ state—possibly with a beginning conversion into the $S=1/2$ state. Unfortunately, the magnetic properties of the metastable isomer **Fe5-NO** × **MeOH(2)** are unknown. In case of **Fe4-NO** × **MeOH** the phase change into the $S=1/2$ state should be nearly complete.

Selected atom distances and angles within the first coordination sphere are listed in Table 6 (for the macrocycles) and Table 7 (for the open-chain complexes). For comparison, some data from literature are included: the macrocyclic complex **FeMe₄TAA-NO** [7c] and both phases of the T -dependent spin conversion of **FeSalen-NO** (1) (taken at r.t.) and (2) (taken at

-175°C) [7b]. The atom numbering in the Tables corresponds with the one given in Fig. 6. Fig. 7 shows the molecule structures (including the one of **FeMe₄TAA-NO**), all approximately in the same projection of the basic chelate complex (the atom numbering in the pictures is that of the original files and may differ from that in the Tables).

In Table 8, some—still unpublished [42,44]—structural data for several iron(II/III) complexes are listed which are derived from the same or very similar equatorial ligands as the nitrosyl derivatives described in this paper. Additional data are published for sixteen iron complexes of type **I** and one iron(II) complex type **II** in [12d,16c,16d,43]. If the atomic distances and angles around the iron would be influenced by the spin state, the oxidation step and the coordination number, the comparison with such base complexes should be helpful to elucidate the binding mode of NO in the nitrosyl derivatives.

The central atom in the macrocyclic nitrosyl derivatives has an approximately square-pyramidal coordination and is located above the plane of the four nitrogen atoms. The average Fe–N_{eq} distance within the macrocyclic framework is for **Fe3-NO** (1.942 Å) and **FeMe₄TAA-NO** (1.944 Å) slightly longer than for **Fe1-NO** (1.924 Å) and **Fe2-NO** (1.925 Å), but the differences are within the standard deviation of the average 1.934(0.020) Å for all sixteen individual bonds in all four complexes. The nitrosyl group points in all four structures towards the six-membered chelate ring of the macrocycle as shown in Fig. 7. The Fe–N–O plane is nearly vertical to the N₄ plane and the Fe–N bond is approximately straight up to this plane. The macrocycle in **Fe3-NO** has the typical saddle shaped distortion of the most dibenzo-tetraaza[14]annulenes [41] but on the non-methylated side of the ligand in a lower extent as in **FeMe₄TAA**.

In the case of the macrocyclic base complexes **I**, the average atom distances Fe–N_{eq} depend hardly on the oxidation step, the spin state and the coordination number of the iron. The average amounts 1.904(0.012) Å for 21 derivatives of **Fe1**, **Fe2** and **Fe3** involving three planar or 4+1 coordinated ($S=1$; Fe–N_{eq}(avg.) = 1.902 Å) and two octahedral ($S=0$; Fe–N_{eq}(avg.) = 1.917 Å) iron(II) complexes, two square-pyramidal pentacoordinated iron(III) halide derivatives ($S=3/2$; Fe–N_{eq}(avg.) = 1.914 Å) and fourteen octahedral adducts in the iron(III) state ($S=1/2$; Fe–N_{eq}(avg.) = 1.901(0.011) Å) with neutral, anionic, and mixed axial ligands. The only exception is the μ -oxo-iron(III) complex $[(\text{Fe3})_2\text{O}(\text{H}_2\text{O})]_2$ with an average Fe–N_{eq}-distance of 2.033 Å. No conclusions about the binding mode of the NO in the nitrosyl derivatives can be drawn by comparison of these Fe–N_{eq} distances. However, considering additionally the displacement of the central atom from the [N₄] plane (0.38; 0.35; 0.44 and 0.39 Å for

Fe1–NO, **Fe2–NO**, **Fe3–NO** and **FeMe₄TAA–NO**, respectively), the only satisfactory relation is found to the $S = 3/2$ halides **Fe1–Cl** (0.405 Å) and **Fe–I** (0.343 Å). Although this is not a strict proof, there is also no contradiction against the assumption that an anionic NO^- is bound in its $S = 1$ state and antiferromagnetically coupled to iron(III) in its intermediate ($S = 3/2$) state.

The nitrosyliron complexes with open-chain ligands, **Fe4–NO** to **Fe6–NO**, show a more diverse behaviour (Table 7)—in the same way as their base iron(II/III) complexes (Table 8). According to their different spin states, the complex **Fe4–NO** × **MeOH** (dominant $S = 1/2$) has significantly lower Fe–L_{eq} distances (average 1.942 Å; nearly the same as for the macrocycles) than

the more electron-withdrawing substituted complex **Fe5–NO** × **MeOH(1)** ($S = 3/2$; average Fe–L_{eq} = 2.016 Å). In the metastable isomer of the latter complex, **Fe5–NO** × **MeOH(2)** (the magnetism of which is unknown), the Fe–L_{eq} distances are more lengthened up to a surprisingly big average of Fe–L_{eq} = 2.064 Å. This can be understood as a trend to lower transfer of electron density from iron to NO. Thus, a formulation as $[\text{Fe}^{\text{II}}\text{L–NO}]$ with antiferromagnetically coupled high-spin iron(II) ($S = 2$) and neutral NO ($S = 1/2$) becomes more relevant. This interpretation is in agreement with the loose binding of nitric oxide, that is eliminated (reversibly) from these complexes in solution in absence of an excess of NO.

Table 8

Bond lengths (Å) and -angles (°) within the first coordination sphere of iron(II/III) complexes type **I** and **II** with different coordination number CN and spin state S (unpublished data [42,44])

Macrocyclic complexes type I

Complex	CN	S	Fe–N _{1,2} ^a	Fe–N _{3,4} ^a	averageFeL _{eq}	Fe–L _{ax}	Fe–pl _{eq} ^b
Fe ^{II} 1	4+1	1	1.877 1.879	1.907 1.908	1.893	2.702	0.077
Fe ^{II} 1 × MeOH	4+1	1	1.879 1.906	1.915 1.906	1.902	2.329	0.110
Fe ^{II} 2 ^c	4	1	1.912 1.836	1.864 2.036	1.911		
Fe ^{II} 2(Py) ₂	6	0	1.917 1.904	1.925 1.932	1.920	2.018 2.037	0.017
Fe ^{III} 1–Cl	5	3/2	1.909 1.912	1.920 1.948	1.922	2.262	0.405
[Fe ^{III} 2(Py) ₂] [⊕]	6	1/2	1.893 1.887	1.909 1.918	1.902	2.022 2.040	0.015
[Fe ^{III} (CN) ₂] [⊖]	6	1/2	1.910 1.902	1.931 1.930	1.918	2.002 2.004	
[Fe ^{III} 1(NCS) ₂] [⊖]	6	1/2	1.896 1.892	1.923 1.926	1.909	1.947 1.954	0.003
[Fe ^{III} 3(NO ₂) ₂] [⊖]	6	1/2	1.908 1.849	1.901 1.912	1.893	1.962 ^d 1.995	0.032
[Fe ^{III} 2(NO ₂)(OH ₂)]	6	1/2 ⇌ 3/2	1.895 1.904	1.925 1.927	1.913	1.963 2.055	0.018
{[(Fe ^{III} 3) ₂ O × H ₂ O]} ₂ ^e	5	5/2? 3/2?	2.025 2.020	2.046 2.042	2.033	1.777	0.589

Complexes type II with Schiff base-like open-chain ligands

Complex	CN	S	Fe–N _{1,2} ^a	Fe–O _{1,2} ^a	Average Fe–L _{eq}	Fe–L _{ax}	Fe–pl _{eq} ^b	Angle O _{eq} FeO _{eq}
Fe ^{II} 6a(HIm)	5	2	2.074 2.097	1.995 1.999	2.041	2.115	0.379	101.5
Fe ^{II} 6a(Him) ₂	6	0 ^f	1.903 1.895	1.943 1.960	1.925	2.014 2.017	0.005	88.2
Fe ^{II} 6a(Py) ₂ (180 K)	6	0	1.923 1.918	1.962 1.955	1.940	2.023 2.025	0.016	92.4
Fe ^{II} 6a(Py) ₂ (290 K)	6	2	2.062 2.053	1.990 2.017	2.031	2.256 2.195	0.027	106.3
Fe ^{II} 6a(MeOH) ₂	6	2 ^g	2.102 2.110	2.031 2.035	2.070	2.223 2.219	0.006	110.7
Fe ^{II} 6b(Py) ₂	6	2	2.105	2.042	2.074	2.271		114.4
Fe ^{II} 6b(MeOH) ₂	6	2	2.097	2.023	2.060	2.267		111.1
Fe ^{II} 7b(Py) ₂	6	2	2.124	2.077	2.101	2.230		116.4
Fe ^{II} 4(Py) ₂	6	2	2.109 2.104	2.049 2.043	2.076	2.256 2.233	0.053	112.1
Fe ^{II} 4(MeOH) ₂	6	2	2.067 2.056	2.026 2.010	2.040	2.246 2.249	0.007	103.3
Fe ^{III} 6a–Cl	5	5/2	2.045 2.046	1.925 1.921	1.984	2.205	0.573	90.9
Fe ^{III} 6a–Br	5	5/2	2.060 2.062	1.934 1.925	1.995	2.351	0.560	92.0
Fe ^{III} 6a–Cl(MeOH)	6	5/2	2.063 2.068	1.951 1.960	2.011	2.273 2.197	0.198	104.6
Fe ^{III} 6–Cl(MeOH)	6	5/2	2.050 2.083	1.977 1.958	2.017	2.285 2.148	0.191	105.8
[(Fe ^{III} 6a) ₂ O] ^h	5	?	2.075 2.072	1.961 1.964	2.018	1.775 1.779	0.587 0.591	93.3

^a Designation according to Fig. 6.

^b Displacement of the iron from the main plane of the equatorial donor atoms.

^c Mixed crystals with the free ligand.

^d Average of 1:1 disordered molecules.

^e Average of distances for four iron atoms.

^f Sharp and strongly reversible spin crossover ($S = 0 \leftrightarrow S = 2$) with small hysteresis at 328 K [28].

^g Cooperative magnetic behaviour with spontaneous magnetisation < 10 K, caused by strong intermolecular H-bridges between R² and MeOH: B.R. Müller, G. Leibel, E.-G. Jäger, Mol. Cryst. Liq. Cryst. 334 (1999) 389.

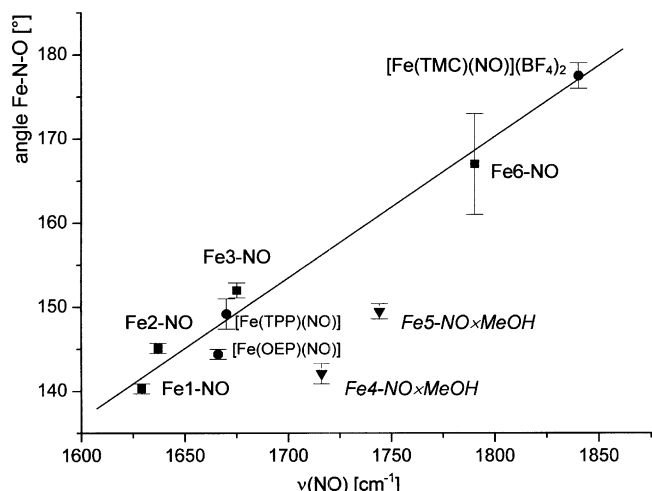


Fig. 8. Correlation between the NO stretching frequencies and the angles Fe–N–O in pentacoordinated nitrosyliron complexes with tetradentate equatorial chelate ligands. The octahedral derivatives **Fe5–NO × MeOH** and **Fe4–NO × MeOH** (italic) are not included into the calculated line. (The equation of the linear fit is 'angle (°) = 0.165 $\nu_{\text{NO}}/\text{cm}^{-1}$ – 128' with $R = 0.987$).

A very indicative structural feature for the spin state of octahedral iron(II) complexes with tetradentate open-chain Schiff base ligands is the 'bite', that means the O–Fe–O angle in the equatorial plane. It is about 90° for low spin iron(II) (cf. **Fe^{II}6a(HIm)₂** and the low-temperature form of **Fe^{II}6a(Py)₂** in Table 8) and increases up to about 110° in the octahedral high spin ($S = 2$) derivatives. Indeed, this 'bite' increases from 89.7 to 104.5° going from **Fe4–NO × MeOH** over **Fe5–NO × MeOH(1)** to **Fe5–NO × MeOH(2)**.

With respect to the binding mode of the NO ligand it is also interesting to note, that there exists a highly significant correlation between the angle Fe–N–O and the stretching frequency $\nu_{\text{N=O}}$ of the NO group. This is displayed in Fig. 8 for our pentacoordinated nitrosyl derivatives, completed by some literature data for other pentacoordinated nitrosyliron complexes of the {Fe–NO}₇ type. (Our octahedral derivatives are also depicted, but not included in the correlation). The increase of the angle (from about 140 to nearly 180°), accompanied by an increase of the force constant of the NO bond is expected for a decreasing population of the antibonding π^* orbital, i.e. for a decreasing transfer of electron density from iron(II) to NO. This indicates the strong effect of the equatorial 'controlling' ligands on the NO binding mode and confirms our assumption that the macrocyclic derivatives are best to describe as [Fe^{III}L⁺–NO[–]] whereas in the case of open-chain ligands with electron-withdrawing periphery the formulation [Fe^{II}L–NO[•]] becomes more probability.

We hope to gain deeper insight into the NO binding mode in our complexes and to confirm our assumption taking advantage from Mössbauer and EPR measure-

ments in combination with SCCX α -DFT calculations. This will be the topic of a subsequent paper.

4. Supplementary Material

Further details of the crystal structure investigations are available on request from the director of the Cambridge Crystallographic Data Centre, 12 Union Road, Cambridge CB2 1 EZ, UK (fax: +44-1223-336033; e-mail:deposit@ccdc.cam.ac.uk; www: http://www.ccdc.cam.ac.uk), on quoting the depository number CCSD-180321 (**Fe1–NO**), CCSD-180325 (**Fe2–NO**), CCSD-180322 (**Fe3–NO**), CCSD-180324 (**Fe4–NO × MeOH**), CCSD-181607, (**Fe5–NO × MeOH(1)**) and CCSD-180323 (**Fe5–NO × MeOH(2)**), the names of the authors, and the journal citation.

Acknowledgements

This work was supported by the Deutsche Forschungsgemeinschaft (Sonderforschungsbereich 436 'Metallvermittelte Reaktionen nach dem Vorbild der Natur'). B.W. acknowledges a grant from the Fonds der Chemischen Industrie. The authors would like to thank Dipl.-Ing. Regina Gollmick for the UV–Vis and Dr. Wolfgang Poppitz for the MS measurements.

References

- [1] J. Lancaster (Ed.), Nitric Oxide: Principles and Actions, Academic Press, San Diego, 1996.
- [2] P.L. Feldman, O.W. Griffith, D.J. Stuehr, Chem Eng. News 20 (1993) 26.
- [3] O. Einsle, A. Messerschmidt, P. Stach, G.P. Bourenkov, H.D. Bartunik, R. Huber, P.M.H. Kroneck, Nature 400 (1999) 476.
- [4] B.B. Wayland, L.W. Olson, J. Chem. Soc., Chem. Commun. (1973) 897.
- [5] (a) W.R. Scheidt, M.E. Frisse, J. Am. Chem. Soc. 97 (1975) 17; (b) W.R. Scheidt, P.C. Piciulo, J. Am. Chem. Soc. 98 (1976) 1913.
- [6] (a) L. Cheng, G.B. Richter-Addo, in: K.M. Kadish, K.M. Smith, R. Guilard, (Eds.) The Porphyrin Handbook, Biochemistry and Binding: Activation of Small Molecules, vol. 4, Academic Press, New York, 2000, pp. 219–339; (b) W.R. Scheidt, M.K. Ellison, Acc. Chem. Res. 32 (1999) 350 (and references therein).
- [7] (a) C. Ercolani, C. Neri, J. Chem. Soc. (A) (1967) 1715–1718; (b) K.D. Hodges, R.G. Wollmann, S.L. Kessel, D.N. Hendrickson, D.G. Van Derveer, E.K. Barefield, J. Am. Chem. Soc. 101 (1979) 906; (c) P. Berno, C. Floriani, A. Chiesi-Villa, C. Guastini, J. Chem. Soc., Dalton Trans. (1988) 1409; (d) F.V. Wells, S.W. McLann, S.L. Kessel, D.N. Hendrickson, R.D. Feltham, Inorg. Chem. 21 (1982) 2306; (e) E. König, G. Ritter, J. Dengler, L.F. Larkworthy, Inorg. Chem. 31 (1992) 1196; (f) J. Dengler, E. König, L.F. Larkworthy, G. Ritter, S.K. Sengupta, Hyperfine Interact. 36 (1990) 1443.

- [8] J.H. Enemark, R.D. Feltham, *Coord. Chem. Rev.* 13 (1974) 339.
- [9] C. Hauser, T. Glaser, E. Bill, T. Weyhermüller, K. Wieghardt, *J. Am. Chem. Soc.* 122 (2000) 4352.
- [10] K.J. Haller, P.C. Johnson, R.D. Feltham, J.H. Enemark, J.R. Ferraro, L.J. Basile, *Inorg. Chim. Acta* 33 (1979) 119.
- [11] E.-G. Jäger, G. Schlenvoigt, B. Kirchhof, M. Rudolph, R. Müller, *Z. Anorg. Allg. Chem.* 485 (1982) 173.
- [12] (a) E.-G. Jäger, E. Stein, F. Gräfe, W. Schade, *Z. Anorg. Allg. Chem.* 526 (1985) 15;
(b) E.-G. Jäger, H. Keutel, M. Rudolph, B. Krebs, F. Wiesemann, *Chem. Ber.* 128 (1995) 503;
(c) E.-G. Jäger, H. Hähnel, H.F. Klein, A. Schmidt, *J. Prakt. Chem.* 333 (1991) 423;
(d) H. Keutel, I. Käßlinger, E.-G. Jäger, M. Grodzicki, V. Schünemann, A.X. Trautwein, *Inorg. Chem.* 38 (1999) 2320.
- [13] E.-G. Jäger, in: L. Fabbri, A. Poggi (Eds.), *Chemistry at the Beginning of the Third Millennium*, Springer-Verlag, Berlin, 2000, pp. 103–138.
- [14] (a) E.-G. Jäger, B. Kirchhof, E. Schmidt, B. Remde, A. Kipke, R. Müller, *Z. Anorg. Allg. Chem.* 485 (1982) 141;
(b) E.-G. Jäger, M. Rudolph, R. Müller, *Z. Chem.* 18 (1978) 229;
(c) E.-G. Jäger, K. Schuhmann, H. Görls, *Inorg. Chim. Acta* 255 (1996) 295;
(d) E.-G. Jäger, K. Schuhmann, H. Görls, *Chem. Ber./Recueil* 130 (1997) 1643.
- [15] (a) E.-G. Jäger, J. Knaudt, K. Schuhmann, A. Guba, in: W. Adam (Ed.), *Peroxide Chemistry—Mechanistic and Preparative Aspects of Oxygen Transfer*, Wiley-VCH, Weinheim, 2000, pp. 249–300;
(b) E.-G. Jäger, P. Renner, *Z. Chem.* 18 (1978) 193;
(c) K. Schuhmann, E.-G. Jäger, *Eur. J. Inorg. Chem.* (1998) 2051–2054;
(d) E.-G. Jäger, J. Knaudt, M. Rudolph, M. Rost, *Chem. Ber.* 129 (1996) 1041.
- [16] (a) E.-G. Jäger, E. Häussler, M. Rudolph, A. Schneider, *Z. Anorg. Allg. Chem.* 525 (1985) 67;
(b) E.-G. Jäger, H. Keutel, *Inorg. Chem.* 36 (1997) 3512;
(c) I. Käßlinger, H. Keutel, E.-G. Jäger, *Inorg. Chim. Acta* 291 (1999) 190;
(d) H. Görls, E.-G. Jäger, *Cryst. Res. Technol.* 26 (1991) 349;
(e) E.-G. Jäger, in: A.X. Trautwein (Ed.), *Bioinorganic Chemistry* (Deutsche Forschungsgemeinschaft), Wiley-VCH, Weinheim, 1997, pp. 584–605;
(f) M. Rudolph, Dissertation (Ph.D. Thesis), Universität Jena, Jena, Germany, 1980.
- [17] M. Rudolph, S. Dautz, E.-G. Jäger, *J. Am. Chem. Soc.* 122 (2000) 10821.
- [18] Y. Numata, K. Kubokura, Y. Nonaka, H. Okawa, S. Kida, *Inorg. Chim. Acta* 43 (1980) 193.
- [19] (a) Autorenkollektiv: *Organikum*, Berlin, 1986;
(b) B. Heyn, B. Hipler, G. Kreisel, H. Schreer, D. Walter, *Anorganische Synthesechemie*, vol. 2, Springer, Heidelberg, 1986.
- [20] K. Müller, E.-G. Jäger, *Z. Allg. Anorg. Chem.* 577 (1989) 195.
- [21] E.-G. Jäger, *Z. Chem.* 8 (1968) 470.
- [22] L.C. Dickinson, J.C.W. Chien, *J. Am. Chem. Soc.* 93 (1971) 5036.
- [23] COLLECT, Data Collection Software; Nonius B.V., Delft, The Netherlands, 1998.
- [24] Z. Otwinowski, W. Minor, in: C.W. Carter, R.M. Sweet (Eds.), *Methods in Enzymology: Macromolecular Crystallography*, vol. 276 (Part A), Academic Press, New York, 1997, pp. 307–326.
- [25] G.M. Sheldrick, *Acta Crystallogr.*, A 46 (1990) 467.
- [26] G.M. Sheldrick, *SHELXL-97*, University of Göttingen, Göttingen, Germany, 1993.
- [27] G. Leibel, Dissertation (Ph.D. Thesis), Universität Jena, Jena, Germany, 2002.
- [28] B.R. Müller, G. Leibel, E.-G. Jäger, *Chem. Phys. Lett.* 319 (2000) 368 (This paper—unauthorized submitted by our former coworker B. Müller—presents preliminary results and contains some mistakes. So, the composition of the imidazole adduct showing the sharp spin crossover is given as $\text{Fe}_6\text{a}(\text{HIm})_{1,8}$ instead of the correct formulation with 2 HIm; the high spin state is written as $S = 3/2$ instead of $S = 5/2$, the fundamental literature is not cited. However, the qualitative description of the cooperative spin crossover in principle meets the reality).
- [29] D.M.P. Mingos, *Inorg. Chem.* 12 (1973) 1209.
- [30] C.A. Brown, M.A. Pavlovsky, T.E. Westre, Y. Zhang, B. Hedman, K.O. Hodgson, E.I. Solomon, *J. Am. Chem. Soc.* 117 (1995) 715 (and references therein).
- [31] A.F. Holleman, N. Wiberg, *Lehrbuch der Anorganischen Chemie*, 101. Auflage, W. de Gruyter, Berlin, 1995, p. 1663, fn 65.
- [32] I. Käßlinger, Dissertation (Ph.D. Thesis), Universität Jena, Jena, Germany, 2002.
- [33] M. Rudolph, S.W. Feldberg, *DIGSIM 3.0*; Bioanalytical Systems Inc., West Lafayette, IN 47906.
- [34] M. Rudolph, in: I. Rubinstein (Ed.), *Physical Chemistry: Principles, Methods and Applications*, Marcel Dekker, New York, 1995.
- [35] E.-G. Jäger, M. Rudolph, *J. Electroanal. Chem.* 434 (1997) 1.
- [36] G.M. Larin, W.W. Minin, E.-G. Jäger, P. Renner, *Koord. Chim.* 4 (1978) 1569.
- [37] K. Pohl, K. Wieghardt, B. Nuber, J. Weiss, *J. Chem. Soc., Dalton Trans.* (1987) 187–192.
- [38] A. Earnshaw, E.A. King, L.F. Larkworthy, *J. Chem. Soc. A* (1969) 2459.
- [39] B.J. Kennedy, A.C. McGrath, K.S. Murray, B.W. Skelton, A.H. White, *Inorg. Chem.* 26 (1987) 483.
- [40] (a) P. Gülich, A. Hauser, H. Spiering, *Angew. Chem.* 106 (1994) 2109;
(b) P. Gülich, A. Hauser, H. Spiering, *Angew. Chem., Int. Ed. Engl.* 33 (1994) 2024 (and references therein).
- [41] (a) F.A. Cotton, J. Czuchajovska, *Polyhedron* 9 (1990) 2553;
(b) P. Mountford, *Chem. Soc. Rev.* 27 (1998) 105.
- [42] E.-G. Jäger, H. Görls, I. Käßlinger, G. Leibel, B. Weber, unpublished results, cf. [27,32] and B. Weber, Dissertation (Ph.D. Thesis), Universität Jena, Jena, Germany, 2002.
- [43] (a) F. Wiesemann, R. Wonnemann, B. Krebs, H. Keutel, E.-G. Jäger, *Angew. Chem.* 106 (1994) 1424;
(b) F. Wiesemann, R. Wonnemann, B. Krebs, H. Keutel, E.-G. Jäger, *Angew. Chem., Int. Ed. Engl.* 33 (1994) 1363.
- [44] W. Imhof, private communication.